Department of Chemistry - Radiochemistry

University of Helsinki

Finland

# Sorption and Diffusion of Se(IV) Species in Crystalline Rock: Experimental studies and Model Development

**Xiaodong Li**

ACADEMIC DISSERTATION

To be presented, with the permission of the Faculty of Science of the University of Helsinki, for public examination in lecture room A129, Department of Chemistry, on 15.10.2021, at 12 noon.

Helsinki 2021

## Supervisors

University lecturer Marja Siitari-Kauppi, PhD

Department of Chemistry – Radiochemistry

University of Helsinki

Helsinki, Finland

Associate Professor Longcheng Liu, PhD

Department of Chemical Engineering,

KTH Royal Institute of Technology

Stockholm, Sweden

## Pre-examiners

Dr. Daniele Pedretti

Department of Earth Sciences, University of Milan

Milan, Italy

Professor Chunli Liu

College of Chemistry and Molecular Engineering, Peking University

Beijing, China

## Opponent

Dr. Sebastien Savoye

Atomic Energy and Alternative Energies Commission, CEA

Paris, France

ISBN 978-951-51-7533-5 (paperback)

ISBN 978-951-51-7534-2 (PDF)

https://ethesis.helsinki.fi

Unigrafia

Helsinki 2021

*"Know what you are doing."*

*"Love what you are doing."*

*"And believe in what you are doing."*

*"Yes, it's just that simple."*

*-Will Rogers*

# Abstract

Bedrock is the final natural barrier providing retention for radionuclides in a spent nuclear fuel repository. The sorption on the pore surfaces of the bedrock and diffusion into the low porous rock matrix are the two most significant processes that retard radionuclides migration through the water-conducting fractures of the crystalline rock.

Se-79 is considered as one of the main contributors to dose-to-man and it has a high impact on the cumulative radioactive dose in a spent nuclear fuel repository. Due to its long half-life and high mobility, sound scientific and technical knowledge are needed to better understand the processes and related mechanisms that determine the Se transport behaviour in bedrock.

Therefore, the focus of this dissertation is on the studies of sorption and diffusion properties of Se(IV) species in bedrock with applications of both experimental and modelling approaches. The results will not only give a deep insight into the mechanisms of Se(IV) retardation in bedrock minerals but also provide convincing data necessary for the safety assessment of spent nuclear fuel deposition.

The work can be divided into two parts, according to the different research objectives. In the first part, the sorption behaviour of Se(IV) species on Grimsel granodiorite and its main minerals, plagioclase, K-feldspar, quartz and biotite were investigated in Grimsel groundwater simulant which has a low ionic strength, in a large Se(IV) species concentration range (from $1.66\times10^{-10}$ M to $1\times10^{-3}$ M). Batch sorption experiments were performed to obtain the distribution coefficients ($K_d$) of Se(IV) species on the rock and mineral samples. Results show that biotite has a much larger specific surface area (SSA) than the other main minerals of granodiorite and the Se sorption on biotite can represent its sorption on the whole bedrock.

Thus, a multi-site surface complexation model for Se(IV) sorption onto biotite was developed based on experimental data from titration and sorption experiments. A batch forward titration coupled with a backtitration method was used to overcome the problem of mineral dissolution in order to measure the reaction constants (pKs) of protonation and deprotonation of sorption sites on surfaces of biotite. Molecular modelling was used to deduce some basic modelling parameters, such as site densities and site types. The technique of PHREEQC coupling with Python was used to calculate and optimize the fitting processes. The model was validated that it can describe the Se(IV) sorption on biotite over pH ranges at least from pH 7.5 to 9.5 which covers most of the pHs of groundwaters deep in the bedrock of a nuclear waste repository.

DFT molecular modelling was performed to provide surface site information and to examine the complexation reactions that happened on the biotite surface. The molecular modelling results showed that two kinds of sorption sites exist on the biotite surfaces; one on the edge surface and the other on the basal surface. The structures of the sorption sites were illustrated at the atomic level. In addition, the surface complexation reactions of different Se species at the two kinds of sorption sites were examined and corresponding sorption energies were calculated.

In the second part of this work, diffusion properties of Se(IV) species in intact rock core were investigated by an updated electromigration device and modelling analysis. The traditional

electromigration device was updated by the introduction of a potentiostat to impose a constant voltage difference over the rock sample and by stabilizing the pH of the background electrolytes.

To interpret the experimental results with more confidence, an advection-dispersion model was developed by accounting for the most important mechanisms governing the movement of the tracer ions, i.e. electromigration, electroosmosis and dispersion. In addition, a reactive transport model was developed based on the consideration that the effects of aqueous chemistry should not be neglected in the former models. The newly developed models, compared to the traditionally used ideal plug-flow model, can provide more precise diffusion parameters. The advection-dispersion model gives nearly the same estimations of parameters as the reactive transport model, with only minor differences in the mean values and uncertainties.

# Acknowledgements

The thesis was finished within the RIP team in the Radiochemistry Unit, Department of chemistry, University of Helsinki. The grant from China Scholarship Council (grant No. 201508110216) is the main financial support for the completion of the thesis work. Additional supports from the Doctoral Programme in Chemistry and Molecular Science for dissertation completion and travel grants are gratefully acknowledged.

During the years of my PhD studies, so many people have entered my life and left a deep impression on my mind. But no one has impressed me as deep as my supervisor, Marja Siitari-Kauppi (Maikki). From the first day I arrived in Helsinki, Maikki has been giving me all her selfless support, guidance and encouragement. You have placed your trust in me to grow into a research scientist and guided me to work independently in planning and executing scientific work. The freedom you gave me to develop my own scientific interests has encouraged me to grow up both as an experimenter and modeller, which opened two bright doors in my life. Your rigorous and serious working attitudes have guided me to be a diligent and serious scientist which I will practice for the whole life. At the same time, your optimistic attitudes towards life ignited my passion, both in work and normal lifetime, even under the seemingly endless coronavirus situations. I admire you for your good temper and everlasting patience and thus the relaxed working environment you have built for us. Please accept my deepest gratitude Maikki!

I also would like to express my most sincere gratitude to professor Longcheng Liu who is also my second supervisor from KTH, Sweden. You have opened the door of modelling and encouraged me to walk bravely with my own wish. Your encouragement is like the precious rain for a long-dried land and helped me go out of the confusion of my life at that time. Your inspiring thinking can always impress me. From you, I learned the importance of multi-discipline and innovative thinking. For me, sometimes, you are like a father who would like to share your life experience and try to guild me on the right road. Sometimes you are like a knowledgeable professor who will teach me with your eternal knowledge. Thanks for teaching me both precious knowledge and experience.

I would also like to express my greatest gratitude to professor Jukka Lehto and professor Daqing Cui. You both worked together to give me the opportunity to study at this famous university and give me the possibility to work in the field of radiochemistry. I must confess that a lot of the ideas in this thesis are initially from you two. Your knowledge and guidance really expanded my knowledge horizons and inspired my thinking throughout my work. I sincerely doubt would I be here without help from you two.

I would like to express my sincere thanks to all my colleagues in RIP team, Jussi Ikonen, Juuso Sammaljärvi, Eini Puhakka, Otto Tikkenen, Noora Pakkanen, Mikko Voutilainen, Jukka Kuva. Special thanks to Jussi Ikonen who is my best Finnish friend. Thanks to tell me so many fascinating stories about Finland and help me know about the Finnish culture. And also special thanks to Eini Puhakka for giving your hand to my studies and research. Without your skills and help, a lot of the work listed in this thesis can not be finished. Also many thanks to Juuso Sammaljärvi who helped me a lot with mineral and rock characterization works.

A lot of thanks are given to people in the Radiochemistry Unit. I thank everyone for your help and kindness. Because of that my research has been going on such well. Many thanks to

professor Gareth Law for taking care of my XAS application to Diamond, especially after three failed trials. Your serious research attitude and writing styles really impressed me and I will benefit from working with you for my whole life. And also thanks for taking care of the dissertation-related procedures. I am greatly thankful to our badminton team members, Surachet Imlimthan, Valtteri Suorsa, Wenzhong Zhang, Junhua Xu. Together we have so many joyful memories to remember. Special thanks to Miho Otaki who helped me with Finnish learning and helped me get out of the complicated Finnish grammars. A lot of thanks to Gianni Vettese, Eliza Lambidis, Joyce Ang and so many others for helping me in my works and life here.

I also would like to acknowledge my colleagues in KTH, Sweden, professor Emeritus Ivas Neretnieks, professor Emeritus Luis Moreno, Shuo Meng, Xiaolei Bian, Zhi Zou. Special thanks to professor Emeritus Ivas Neretnieks for your valuable advice which helped me develop the coupling process between models. I admire your knowledge and wisdom. Many thanks to all of you and I hope all my best to you.

I will not forget the joyful moments together with the Chinese community in Kumpula, Zhongmei Han, Junhua Xu, Wenzhong Zhang, Hangzhen Lan, Chao Zhang, Ming Guo and all the others. Because of you, the winter in Finland is not long at all, but colourful and joyful.

At last, I would like to give my best gratitude to my parents. Forgive me that I can only visit you once a year. I always feel bad when thinking that I can not company you more time and help you with more homework. But my love for you is even stronger with a longer distance. I really grateful for giving me such kind education and a harmonious family. I only hope I didn't disappoint you two. I just want to say I LOVE YOU.

Helsinki, March 2021

Xiaodong Li

# List of Publications

1. **Li, X.**, Puhakka, E., Ikonen, J., Söderlund, M., Lindberg, A., Holgersson, S., Martin, A., Siitari-Kauppi, M., 2018. Sorption of Se species on mineral surfaces, part I: Batch sorption and multi-site modelling. Applied Geochemistry 95, 147–157. https://doi.org/10.1016/j.apgeochem.2018.05.024

2. Puhakka, E., **Li, X.**, Ikonen, J., Siitari-Kauppi, M., 2019. Sorption of selenium species onto phlogopite and calcite surfaces: DFT studies. Journal of Contaminant Hydrology 227, 103553. https://doi.org/10.1016/j.jconhyd.2019.103553

3. **Li, X.**, Puhakka, E., Liu, L., Zhang, W., Ikonen, J., Lindberg, A., Siitari-Kauppi, M., 2020. Multi-site surface complexation modelling of Se(IV) sorption on biotite. Chemical Geology 533, 119433. https://doi.org/10.1016/j.chemgeo.2019.119433

4. **Li, X.**, Meng, S., Puhakka, E., Ikonen, J., Liu, L., Siitari-Kauppi, M., 2020. A modification of the electromigration device and modelling methods for diffusion and sorption studies of radionuclides in intact crystalline rocks. Journal of Contaminant Hydrology 231, 103585. https://doi.org/10.1016/j.jconhyd.2019.103585

5. Meng, S., **Li, X.**, Siitari-Kauppi, M., Liu, L., 2020. Development and application of an advection-dispersion model for data analysis of electromigration experiments with intact rock cores. Journal of Contaminant Hydrology 231, 103618. https://doi.org/10.1016/j.jconhyd.2020.103618

Author's contributions:

1. X. Li and J. Ikonen conceived the research. X. Li conducted all the experiments except for the HPLC-ICP-MS measurements which were conducted with the help of M. Söderlund. X. Li and E. Puhakka performed the modelling of the experimental data together. A. Martin provided the rock samples. A. Lindberg performed XRD measurements and S. Holgersson performed SSA measurements of the rock samples. X. Li wrote the manuscript. M. Siitari-Kauppi supervised the working process and commented on the manuscript.

2. E. Puhakka, J. Ikonen and X. Li conceived the research. E. Puhakka performed DFT modelling while X. Li performed experiments and SCM modelling. E. Puhakka and X. Li wrote the manuscript and X. Li was the corresponding author of the article. Siitari-Kauppi supervised the working process and commented on the manuscript.

3. X. Li and E. Puhakka conceived the research. X. Li conducted all the experiments with the help of W. Zhang for Se concentration measurements and A. Lindberg for XRD

measurements. X. Li and E. Puhakka performed modelling of the experimental data. L. Liu helped the development of the coupling between different models. X. Li and E. Puhakka wrote the manuscript. M. Siitari-Kauppi and L. Liu supervised the working process and commented on the manuscript.

4. X. Li and S. Meng conceived the research. X. Li and S. Meng conducted the experiments. L. Liu, X. Li and S. Meng performed the development of the new models for electromigration results. E. Puhakka performed molecular modelling to help with illustration of the experiment results. X. Li wrote the manuscript. M. Siitari-Kauppi and L. Liu supervised the working process and commented on the manuscript.

5. S. Meng and X. Li conceived the research. S. Meng, L. Liu and X. Li performed the development of the two new models. X. Li and S. Meng conducted the experiments and SCM modelling. S. Meng and X. Li wrote the manuscript. L. Liu and M. Siitari-Kauppi supervised the working process and commented on the manuscript.

# Abbreviations

| | |
|---|---|
| 2SPNE SC/CE | 2 site protolysis non-electrostatic surface complexation and cation exchange |
| AD | advection-dispersion model |
| CCM | constant capacitance model |
| CASTEP | CAmbridge Serial Total Energy Package |
| CEC | cation exchange capacity |
| $D_e$ | effective diffusion coefficient |
| DFT | density functional theory |
| EDL | electric double layer |
| EPMA | Electron Probe Micro-Analyzer |
| EXAFS | extended x-ray absorption fine structure |
| $F_f$ | formation factor |
| HLW | high-level radioactive waste |
| HPLC | high-performance liquid chromatography |
| IAEA | International Atomic Energy Agency |
| ICP-MS | inductively coupled plasma mass spectrometry |
| IPF | ideal plug-flow model |
| $K_d$ | distribution coefficient |
| Kr-BET | Kr gas adsorption Brunauer-Emmett-Teller model |
| LLNL | Lawrence Livermore National Laboratory |
| NEM | nonelectrostatic model |
| PMMA | poly(methyl methacrylate) |
| RT | reactive transport model |
| SCM | surface complexation model |
| SNF | spend nuclear fuel |
| SSA | specific surface area |
| XAS | X-ray absorption spectroscopy |
| XANES | X-ray Absorption Near-Edge Structure |
| XRD | X-ray Powder Diffraction |

# Contents

# 1 Introduction

Around 11% of the electricity produced worldwide is currently generated from nuclear power (Figure 1, left). About 450 nuclear power plants are operating in 31 countries and 60 more reactors are under construction, accounting for about 15% of the existing capacity (IAEA, 2018a). In 2017, nuclear power plants provided 2487 TWh of global electricity, rising from 2477 TWh in 2016. It can be foreseen that nuclear power will play a more important role over the coming years to meet the global challenge of growing energy demand and low-carbon power generation (Figure 1, right).

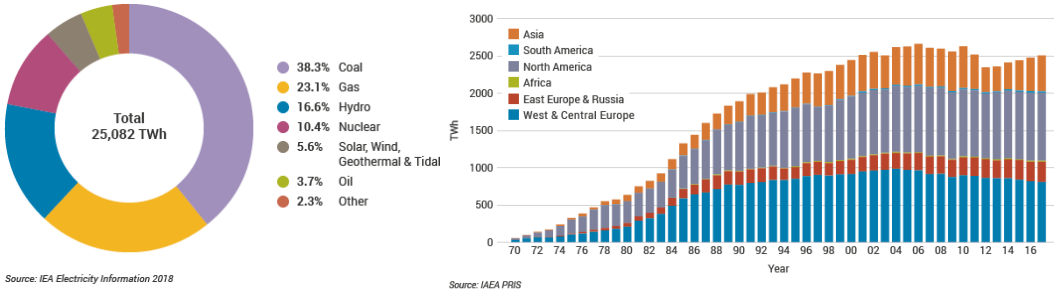


*Figure 1. Electricity produced by different sources worldwide in 2016 (left). Number of operable reactors worldwide (right) (IAEA, 2018a).*

The process of producing electricity from nuclear materials (nuclear fuel cycle) creates high amounts of radioactive spent nuclear fuel (SNF). According to the reports published by the International Atomic Energy Agency (IAEA), the disposal volume of the solid high-level radioactive waste (HLW) inventory is approximately 22,000 $m^3$ (IAEA, 2018b). The long timescales over which some waste remains radioactive has led to the idea of disposal in the deep underground repositories in stable geological formations. Thus, it is critical to understand how the characteristics of SNF evolve with time (Figure 2) and how it affects the storage environment in order to design reliable and safe geological repositories for SNF.

Among the radionuclides in SNF, Se-79 is evaluated as High-priority (II) according to the expectations that it may give a significant contribution to the doses in some biosphere scenarios in the SNF deposition (Hjerpe et al., 2010; Posiva Oy, 2013). Due to its long half-life ($3.1\times10^5$ years) and high mobility in the geological environment, Se-79 is a radionuclide that needs great concern when thinking about the long-term safety of radioactive waste repository (Ewing, 2015; Neall et al., 2007; Siegel and Bryan, 2003). It has a high impact on the cumulative dose in a SNF repository and affects the radioactivity levels for a long time. Thus, detailed studies concerning Se migration behaviours (sorption and diffusion) are essential to assure the long-term safety of SNF under the plans for the disposal of SNF.

In Finland, the KBS-3 concept is used for the long-term geological disposal of SNF. The KBS-3 concept includes several engineering and natural barriers that are designed to isolate the

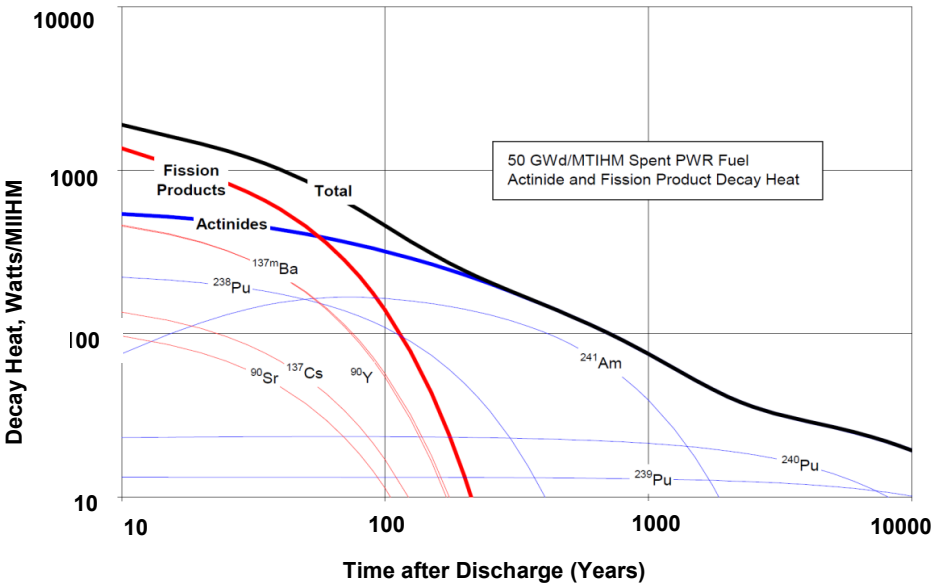


*Figure 2. Dominant decay heat contributors in SNF vs. time (radiotoxicity normalized to natural uranium and decay products as occurs in natural uranium ore) (Wigeland et al., 2004).*

harmful radionuclides from reaching humans and the environment for 100,000 years (Posiva Oy, 2012; SKB, 2013). This is often termed the "multi-barrier" concept (Figure 3). The first barrier, copper canisters, are designed to withstand corrosion and the mechanical forces that can result from movements in the rock surrounding the Spent Fuel Repository. The copper canisters will be surrounded by bentonite clay, which is the second barrier, after placing them in the holes that are located in the tunnels in a horizontal or vertical position. The bentonite clay will act as a buffer and protect the canisters from corrosion and minor movements. The final barrier is the surrounded bedrock in-depth (about 500 m) which provides a stable chemical and physical environment. If any radioactive substances were to escape from a canister and penetrate through the bentonite clay buffer, they could be caught by surfaces and minerals in the bedrock fractures and the rock's pores by chemical sorption and matrix diffusion (Smith et al., 2007).

In Finland, the nuclear fuel repository is being built at Olkiluoto, the bedrock of which is composed of crystalline granite. By comparing the sorption behaviours of Se(IV) species on the composed minerals of granite, Yang et al. (2018) concluded that biotite can be representative of the Se(IV) sorption in the granite mineral assemblages. Thus, the biotite contents are critically important to evaluate the migration of Se(IV) species in granite. In the scenario that radionuclides have escaped the repository and are released into the groundwater, the most significant processes of delaying radionuclides from the flowing fracture water through bedrock fractures are their sorption onto the mineral surfaces and diffusion into the rock matrix. Therefore, the sorption properties of Se(IV) species on granite bedrock, especially on biotite, and the diffusion properties when they are migrating in the bedrock, have to be carefully determined for the safety assessment of the final disposal.

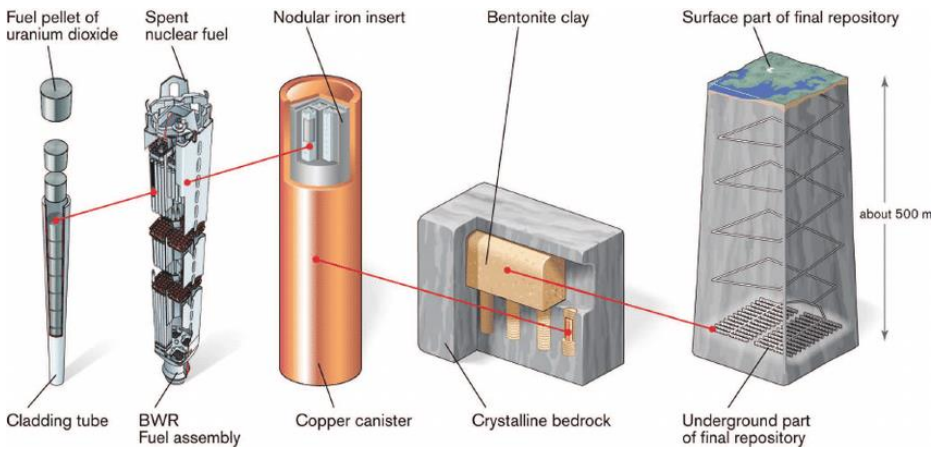


*Figure 3. The KBS-3 method that includes several natural and engineering barriers termed the "multi-barrier" concept (SKB, 1999).*

The aim of this thesis is to develop new techniques for studying the sorption and diffusion behaviours of Se(IV) species through both experimental and modelling approaches. The sorption properties of Se(IV) species, described as distribution coefficients, $K_d$, on Grimsel granite and its main minerals, including plagioclase, K-feldspar, quartz and biotite, were investigated by batch sorption approaches (**Paper 1**). The results confirmed our assumption that the Se(IV) sorption on biotite surfaces can be representative of bulk Se sorption to complex mineral assemblages. Thus, sorption studies of Se on biotite are crucial to evaluate the Se mobility in the groundwater system. To better illustrate the Se(IV) sorption behaviour and provide an approach to predict its environmental distributions, a multi-site surface complexation model for Se(IV) sorption on biotite was developed based on three sets of experimental data: titration data, sorption edge data and sorption isotherm data (**Paper 2**). In this model, we proposed that at least one kind of strong sorption site and two kinds of weak sorption sites, exist on biotite surfaces. In order to explain experimental results, we also proposed that different sorption complexation reactions occur between Se(IV) species and the different sorption sites relative to different environmental pH conditions. The model was validated that it can provide quantitative predictions of Se(IV) sorption in groundwater conditions of a deep geological repository. To find theoretical supports for our model predictions, we performed DFT molecular modelling by solving the total electronic energy and overall electronic density distributions to define energetically stable structures for biotite and sorbed Se(IV) species (**Paper 3**). Two types of sorption sites were investigated, one sited on the (001) basal surface and the other on the (110) edge surface. Those sites were identified as the two kinds of weak sorption sites in surface complexation modelling. The sorption geometries between the sorption sites and Se(IV) species were also calculated. According to the modelling process, electron transfer reactions happen between the biotite surface and Se(IV) species when coordination reactions happen on the (110) edge surface, and during the reaction

processes, anionic and neutral Se(IV) species can transfer to cationic species $HSeO_2^+$. In contrast, at the (001) basal surface, electron transfer processes are not thought to be dominant.

The diffusion properties of Se(IV) species, described by effective diffusion coefficient, $D_e$, was measured by a modified electromigration device (**Paper 4**). The new electromigration device used in this work was modified, based on the traditional electromigration device, by introducing a potentiostat to impose a constant voltage over the studied rocks sample and stabilizing the background solution pH conditions. The results show that the modified electromigration device can give more stable and accurate experimental results than those from the traditional electromigration device. To interpret the electromigration experimental results with more confidence, an advection-dispersion model and a reactive transport model were developed in this thesis (**Paper 5**). Compared with the traditionally used ideal-plug flow model which only takes into account electromigration effects, the newly developed models take into account more effects that can affect the experimental results, including electromigration, electroosmosis and dispersion. The results show that the new models can provide better parameter identifications with smaller uncertainties than the traditionally used ideal plug-flow model.

# 2 Background

## 2.1 Chemistry of Selenium

Selenium has five stable isotopes, $^{74}$Se (80.89%), $^{76}$Se (9.36%), $^{77}$Se (7.63%), $^{78}$Se (23.78%), $^{80}$Se (49.61%) and 26 radioisotopes. $^{79}$Se is one of the most important radioisotopes due to its common existence in SNFs. It is a fission product of $^{235}$U with a low fission yield of 0.044%. However, most $^{79}$Se in SNF are produced from selenium-bearing materials found in nuclear fuel itself and reactor construction materials by the neutron irradiation-induced activation of stable $^{78}$Se reaction, $^{78}$Se (n, $\gamma$) $^{79}$Se (Lehto and Hou, 2011).

The behaviour of radionuclides under the conditions of long-term disposal in a geologic repository depend specifically on their chemical forms. The geochemical mobility of long-lived fission products like $^{79}$Se, as well as actinides such as U and Pu, largely depends on the redox conditions (Cordfunke and Konings, 1988; Ewing, 2015). Oxidation states of redox-sensitive radionuclides have a significant effect on their solubility, transport, bioavailability and toxicity. In general, the reduction of radionuclides to their lower valence states results often in low solubility and an increased tendency to sorb onto mineral surfaces, thus lowering their mobility in the environment (Cronenberg and Osetek, 1987).

The most common oxidation states of selenium under the natural conditions are –II (FeSe, $HSe^-$), -I ($FeSe_2$), 0 (Se(s)), +IV ($SeO_3^{2-}$, $HSeO^{3-}$) and +VI ($SeO_4^{2-}$, $HSeO_4^-$), as shown in Figure 4 (Lehto and Hou, 2011; National Institute of Advanced Industrial Science and Technology, 2005). Se(VI) dominate the selenium species under oxic conditions (> +400 mV) and the most common form is a basic anion, selenate ($SeO_4^{2-}$). At lower redox conditions (< +400 mV), Se(VI) is reduced to Se(IV) and the dominant species in this oxidation state are selenite ($SeO_3^{2-}$) and biselenite ($HSeO_3^-$), depending on the pH conditions (Atwood, 2010). At redox potentials around 200 mV, selenium also exists as elemental selenium (Figure 4). The reduction of selenium is slow and kinetically hindered because it involves the transfer of multiple electrons along with multiple oxygen atoms between its various oxidation states (De Cannière et al., 2010). Under the reducing conditions of a nuclear waste repository, the reduction of selenate is very reluctant in the absence of a catalyst. The kinetics of selenite reduction was studied in detail by Bruggeman et al. (2005). They show that the decrease of Se(IV) species concentration as a function of time seems proportional to the concentration of dissolved selenite and to the amount of solid pyrite, $FeS_2$, present in the system, and inversely proportional to the square root of the $FeS_2$ occupancy by selenite (Equation (1)). These observations suggest that $SeO_3^{2-}$ reduction takes place through sorption onto $FeS_2$ and that a selenium precipitate with a solubility of $3 \times 10^{-9}$ M was formed (Bruggeman et al., 2005; De Cannière et al., 2010).

$$\frac{d[Se(+IV)]}{dt} = -k[Se(+IV)][FeS_2]_0 \sqrt{\frac{[FeS_2]_0}{[Se(+IV)]_0}} \quad (1)$$

The Se oxidation states and speciation analysis were checked by the application of HPLC-ICP-MS (High-performance liquid chromatography connected to an inductively coupled plasma mass spectrometry) in our batch sorption experiments which lasted for about one month. The

results show that no detectable amount of Se(IV) was oxidised to Se(VI) in ambient atmosphere conditions during the experimental time (Li et al., 2020, 2018).

The solubility of selenium in different forms is another important factor that affects its mobility in nature. Under oxidizing conditions, Se(IV) and Se(VI) salts are soluble and very mobile. No solubility limits are reached for $SeO_4^{2-}$ and $SeO_3^{2-}$ in groundwater conditions. If taking into account the reluctant reduction of selenate, it is necessary to consider that selenate is the possible species of Se that migrates in the conditions of the nuclear waste repository. Under reducing conditions, the mobility of selenium is limited by the solubility of poorly soluble elemental selenium Se(0) or iron selenide (FeSe). The reduction and formation of the lower oxidation states of selenium will contribute to delay and attenuate the $^{79}Se$ release from the source term and to spread it over a long time period (Missana et al., 2009).

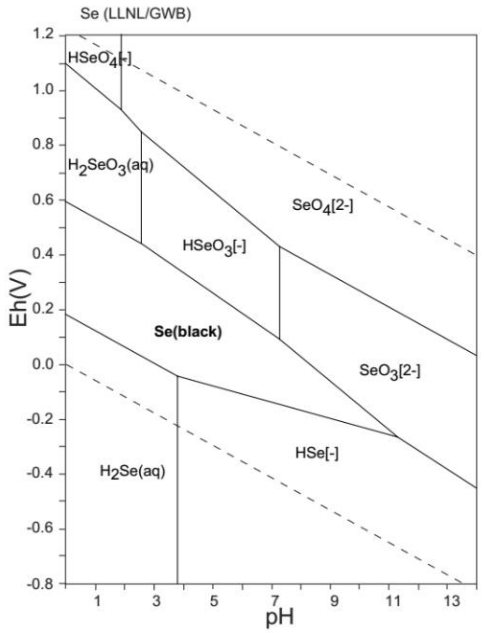


*Figure 4. Eh-pH diagram for selenium calculated from the data of Lawrence Livermore National Laboratory (LLNL) (National Institute of Advanced Industrial Science and Technology, 2005).*

## 2.2 Sorption Process

The clay minerals, organic matter or metal oxy-hydroxides existing in soils and aquifers can sorb chemicals on its surface. In general, the removal of a soluble compound from a solution phase is often identified simply as a sorption process. In this definition, no specific mechanism (adsorption or ion exchange) is implied. However, strictly speaking, adsorption and ion exchange are different processes, as illustrated in Figure 5. Adsorption refers to the adherence of a chemical to the surface of the solid; it suggests that the chemical is taken up into/on the solid. The ion exchange process involves the replacement of one chemical for another one into/on the solid.

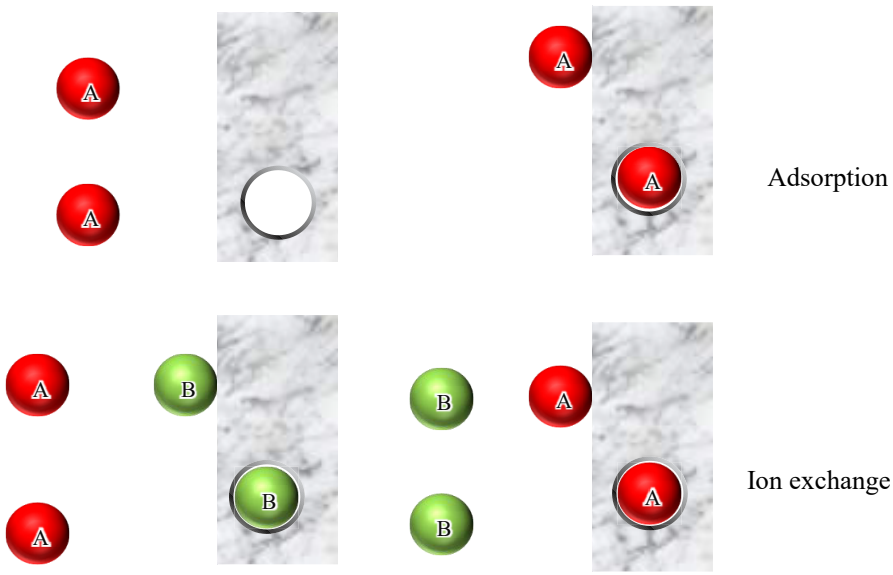


*Figure 5. Schematic illustration of adsorption and ion exchange processes.*

### 2.2.1 Surface charge

The minerals' surfaces are charged which makes them highly reactive and this is the first step to understand the sorption processes in minerals. There are two types of charge on mineral surfaces, permanent and pH-dependent charges. The permanent charge is developed at the time the mineral crystallizes from liquid magma or precipitates from a supersaturated solution. Thus, the permanent charge is a property of the mineral that cannot be altered by the surrounding chemistry of the environment. The development of the permanent charge is a process of isomorphic substitution. For example, the isomorphic substitution of $Al^{3+}$ for $Si^{4+}$ in the tetrahedral layer will result in a deficit of the positive charge required to neutralize the coordinating anion charge. As a result, a negative charge in the mineral structure is created and an interlayer cation must be applied to neutralize the structural charge.

The pH-dependent charge on a mineral is developed by the result of the protonation and deprotonation of surface hydroxyl groups (≡SOH, where ≡S represents a metal-bound in the crystal structure). The pH-dependent charge associated with a surface functional group can be negative, positive and neutral. The most common way to describe the protonation and deprotonation of the inorganic surface functional group is the 2-pK approach which can be shown by the two protolysis reactions below:

$$\equiv SOH + H^+ \rightarrow \equiv SOH_2^+; \qquad K_{a1} \tag{2}$$

$$\equiv SOH \rightarrow \equiv SO^- + H^+; \qquad K_{a2} \tag{3}$$

$K_{a1}$ and $K_{a2}$ are the defined stability constants of the protonation and deprotonation reactions.

In the work, the detailed $K_{a1}$ and $K_{a2}$ values for different sorption sites on biotite surfaces are measured with titration technique and modelled with surface complexation modelling.

A schematic illustration of the biotite surface is shown in Figure 6. Biotite is a group of sheet-like silicate minerals ubiquitous in soils and rocks with the general composition being $K(Mg,Fe)_3(AlSi_3O_{10})(F,OH)$. Recent studies reported the surface properties of silicate minerals are strongly dependent on the aqueous phase compositions (Bray et al., 2014). The reported $pH_{ZPC}$ values of biotite range from 6-7 (Alonso et al., 2009) and the $pH_{IEP}$ values are more various, ranging from 0.41 to over 3 (Bray et al., 2014; James and Healy, 1972). Thus, researchers reported that the sole use of $pH_{ZPC}$ or $pH_{IEP}$ can not provide an accurate depiction of the biotite surface chemistry (Bray et al., 2014). A combined approach of electrokinetic measurements, potentiometric titrations and aqueous solution chemistry analyses has to be performed to provide insight into the interaction of protons with biotite surfaces.

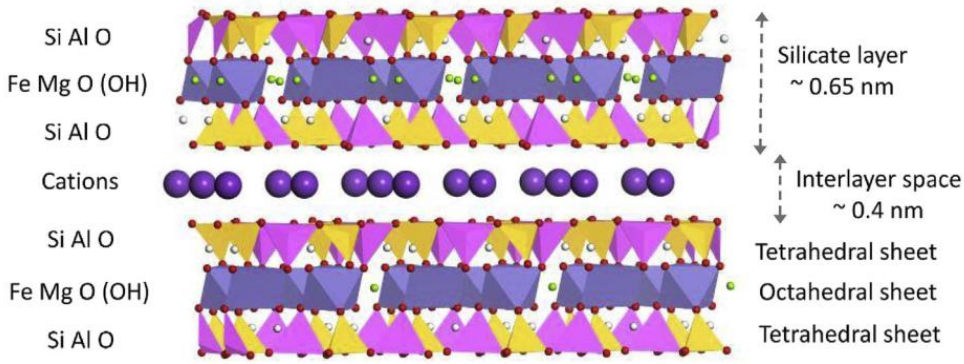


*Figure 6. Schematic illustration of the biotite structures. Tetrahedral sheet: silicon – yellow; aluminium – aniline red. Octahedral sheet: iron – blue; magnetic – green. Interlayer: potassium – purple.*

### 2.2.2 Surface Complexes

A surface complex is formed when a surface functional group reacts with ions or molecules existing in the solution phase. Two types of surface complexes exist on a mineral surface which are inner-sphere and outer-sphere surface complexes, respectivley (Figure *7*, Appelo and Postma, 2004). If there are one or more water molecules between the adsorbed substance (ion or molecule) and a surface ligand, an outer-sphere surface complex is formed. In contrast, an inner-sphere complex is formed when there is no water molecule between a charged surface functional group and the adsorbed substance.

Outer-sphere surface complexes are maintained by electrostatic forces. This sorption mechanism is normally non-specific and the adsorbed substance can be easily displaced from the surface by other substances existing in the solution phase. In contrast, the sorption of a substance by a surface function group by inner-sphere mechanism is specific, which means they

are tightly bound through bonds produced through them with a relatively high degree of structural configuration and covalent character.

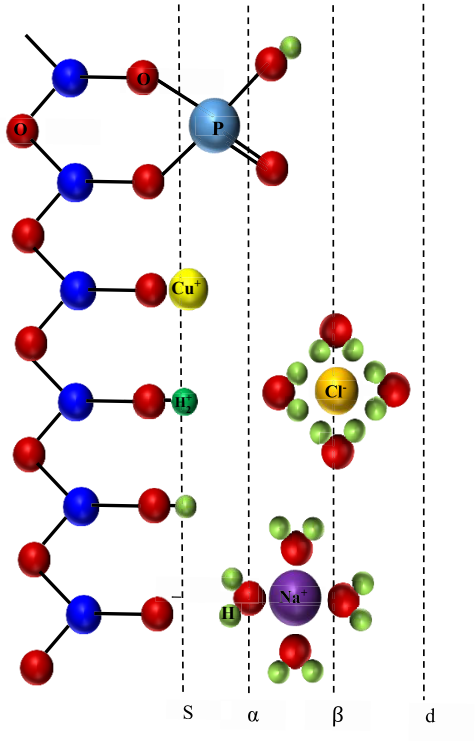


*Figure 7. Schematic illustration of inner-sphere and outer-sphere bonding and ions in the diffuse double layer. "s" for surface hydroxyl groups, "α" for inner-sphere complexes, "β" for outer-sphere complexes and "d" for ions in the diffuse layer (modified from Appelo and Postma, 2004).*

The type of chemical bond formed at the solid-solution interface defines the mechanisms responsible for the retention of substances. The outer-sphere sorption is a direct result of negative (or positive) charge formation on the mineral surface. As shown in Figure 8, the sorption of $Na^+$ (or $NO_3^-$) by a constant potential mineral surface (gibbsite) will increase (or decrease) in a manner consistent with the increasing concentration of negative (or positive) charged surface sites (Essington, 2015). The outer-sphere retention of a sorbent is also easily reversible and decrease with increasing ionic strength.

In contrast, inner-sphere surface complexation by a constant potential mineral surface is generally not tied to the formation of negative (or positive) surface charge. Instead, the sorption increases rapidly from a minimum to a maximum value in a narrow pH range, as indicated by Figure 9 which shows the sorption of $Ni^{2+}$ by quartz, kaolinite and gibbsite as a function of pH from 3 to 10 (Sarkar et al., 2000, 1999). The inner-sphere sorption reactions also tend to be

irreversible and unaffected by ionic strength, indicating a high degree of specific bonding in the surface complexes.

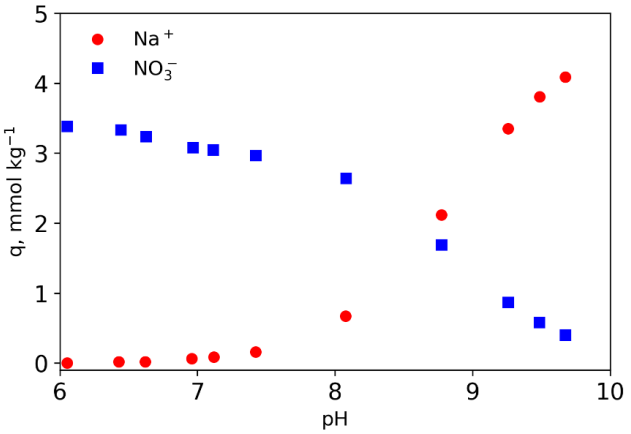


*Figure 8. The sorption behaviour of $Na^+$ and $NO_3^-$ as a function of solution pH (Essington, 2015).*

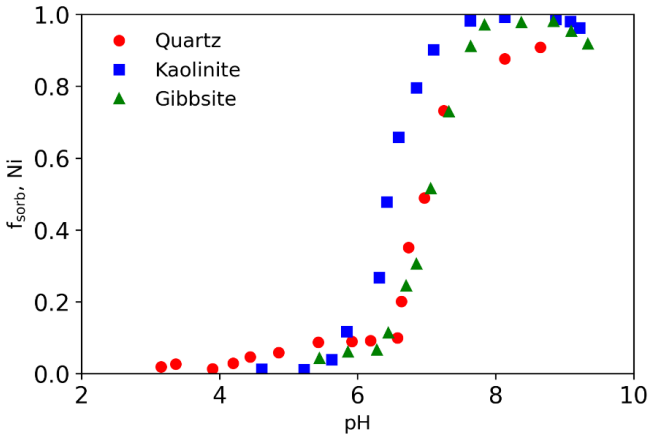


*Figure 9. The fraction of Ni sorbed by quartz, kaolinite and gibbsite as a function of pH (Sarkar et al., 2000, 1999).*

It is commonly thought that Se(IV) species, both selenite or biselenite, tend to form strongly bonded inner-sphere complexes on mineral surfaces or soil organic matter; in contrast, Se(VI) species (mainly selenate) tend to be sorbed in an outer-sphere manner (He et al., 2018; Li et al., 2017). The results were first observed by Hayes et al. (1987) who performed extended x-ray absorption fine structure (EXAFS) measurement of adsorbed selenate and selenite ions at an $\alpha$-FeOOH(goethite)-water interface. They found that the selenite ion is bonded directly to the goethite surface in a bidentate fashion with two iron atoms 3.38 Å from the selenium atom, while selenate has no iron atom in the second coordination shell of selenium, which indicates

retention of its hydration sphere upon sorption. A typical inner-sphere surface complexation sorption edge ($K_d$ ~ pH) experimental results, similar as shown in Figure 9, were observed in our work (Paper 2). A rapid sorption $K_d$ values decrease from pH 4 to 8 of Se(IV) sorption on biotite clearly shows the inner-sphere surface complexation properties.

### 2.2.3 Sorption description

Distribution coefficient ($K_d$) is a general way to describe the sorption of substances quantitatively by soils or minerals. $K_d$ is defined at equilibrium conditions, as the ratio of the amount of sorbed substances per unit mass of sorbent (s, mol/kg etc.) and the amount of substance in solution per unit volume ($c_{eq}$, mol/L etc.).

$$K_d = \frac{s}{c_{eq}} \tag{4}$$

The relationship between sorbed and dissolved solute concentrations at a fixed temperature is called a sorption isotherm. Two equations are often employed to describe the relation, the Freundlich isotherm and the Langmuir isotherm. The Freundlich isotherm has the form:

$$s = K_F \cdot c_{eq}^{n} \tag{5}$$

where $K_F$ and $n$ are adjustable coefficients. Usually, $n$ is less than 1, so that the increase of sorbed concentration lessens as the solute concentration increases.

However, the use of the Freundlich equation tends to be limited, because it shows that the sorption extends infinitely as concentration increases, which is unrealistic. In the real conditions, the quantities of sorption sites are limited which limits the amount of sorbed substances in high concentration conditions. Another observation in sorption experiments is that $K_d$ becomes constant when concentrations are small. The Freundlich equation can not explain this sorption property either. In spite of this, in our work, the Freundlich equation can be used to well describe the Se(IV) sorption behaviours on various rock and mineral samples (Paper 1). The coefficients $K_F$ and $n$ in the Freundlich equation were calculated and summarised.

The Langmuir equation has a better theoretical background and can be derived from the law of mass action in a sorption reaction. The Langmuir isotherm has the form:

$$s = \frac{s_{max}\, c_{eq}}{K_L + c_{eq}} \tag{6}$$

where $s_{max}$ is the maximum amount of sorption sites per mass of sorbent; $K_L$ is a constant related to the affinity of the binding sites.

The Langmuir equation explains the reality of sorption limits at high concentration conditions. According to the Langmuir equation, the sorbed concentration $s$ increases linearly with solute concentration $c_{eq}$, if $c_{eq} \ll K_L$. When the concentration of solute is very high and $c_{eq} \gg K_L$, the surface becomes saturated and $s = s_{max}$.

### 2.2.4 Modelling of sorption processes

#### 2.2.4.1 Electric double layer models

Three types of models are commonly used to describe the structure of the electric double layer of minerals: (a) Helmholtz model; (b) Gouy-Chapman model and (c) Stern triple layer model. A comparison of these three models is shown schematically in Figure 10. The Helmholtz model (Figure 10, a) is the simplest double layer model. The Helmholtz model assumed two layers of charge evenly distributed on both sides of the solid-solution interface. This is also the origin of the name "double layer". The negative charge is assumed to be distributed evenly on the solid surface while the positive counter charge is evenly distributed in the solution layer which is parallel to the solid surface at some distance. The surface potential drops off linearly with the increase of the distance from the solid surface, from the maximum at the solid surface to 0 (bulk solution potential is assumed to be 0). However, this model has an obvious defect. It cannot explain the experimental observation that the relative potential and solution concentration have an impact on the double layer.

The Gouy-Chapman model (Figure 10 b) assumed, same as the Helmholtz model, that the surface is plane and infinite and the negative charge density is evenly distributed over the surface. The difference is that it introduced a new concept called diffuse double layer, which means that counter ions in the solution layer are exposed to a balance between electrostatic and diffusion forces. The diffuse distribution of dissolved cations and anions at the surface is the result of a force balance. The attractive electrostatic force pulls cations toward the surface, resulting in higher cation concentrations in this zone than in the bulk solution. Conversely, the negatively charged surface repels anions from the surface region, resulting in a lower anion concentration than in the bulk solution. At the same time, because of the existence of diffusive force, the cations are pulled away from the surface and also a diffuse force pulls anions into the surface region. When equilibrium is attained, the solution surface layer will extend out away from the surface, with cation concentration and surface potential decreasing with distance and the anion concentration increasing with distance. The thickness of the diffuse double layer ($\kappa^{-1}, m$) can be used to explain phenomena like the diffusive flux and anion exclusion (Dagnelie et al., 2018). It can be defined as:

$$\kappa^{-1} = \frac{3.042 \times 10^{-10}}{ZI^{0.5}} \tag{7}$$

where Z is the counter ion charge and I is the ionic strength. The equation shows that the thickness of the diffuse double layer decreases with the increase of ionic strength and the increase of counter ion valence.

In the Gouy-Chapman model, the charge is abstracted as a point. This is a common assumption in physical models. However, under the condition of large potential difference, the "point charges" will be infinitely compressed to the position close to the electrode surface, resulting in an infinite prediction of capacitance. Thus, in the Stern triple layer model (Figure 10 c), the condition of the size of ions is added. The solution region near the surface is also divided into

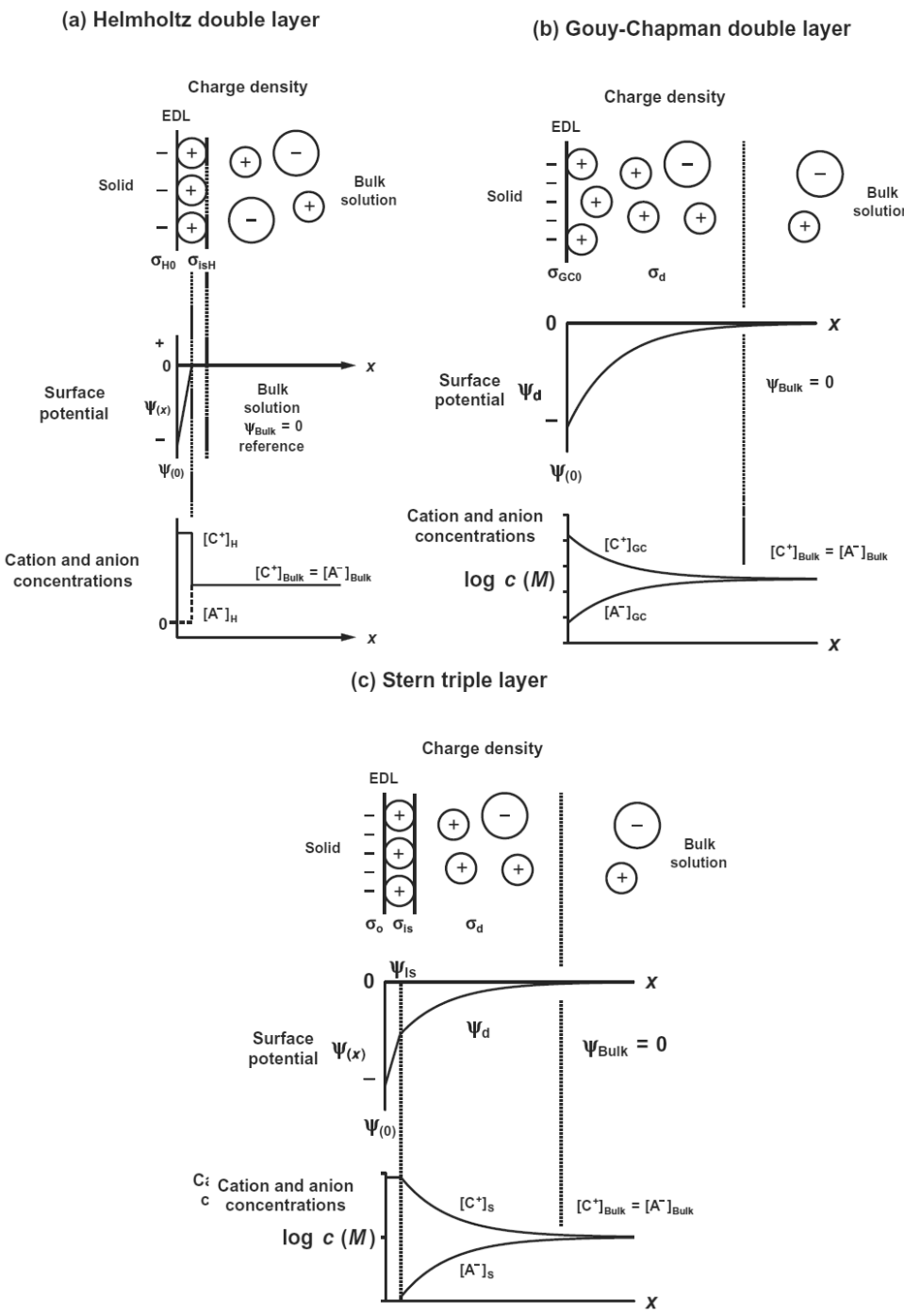


*Figure 10. Electric double layer (EDL) models that describe the solid-solution interface, modified from (Essington, 2015).*

two layers in the Stern triple layer model. In the inner-layer which is close to the surface, ions are specifically adsorbed and form a compact layer of counter ion charge, which is similar to the Helmholtz model. The outer layer is defined the same way as the diffuse double layer. In general, the triple layer model has more options to account for mechanistic details of the sorption processes.

However, Dzombak and Morel (1990) derived a comprehensive database for sorption on ferrihydrite with the Gouy-Chapman double layer model which fits many observations. Thus, the double layer model has become the standard for many sorption modelling in natural environments. Dzombak and Morel's database was also accepted by PHREEQC which is the software we used for surface complexation modelling in our work.

#### 2.2.4.2 Surface complexation models

A surface complexation model (SCM) is a tool to identify the chemical reactions and associated equilibrium constants. If a mechanism is known for the sorption reaction, an SCM can also be employed to determine the specific equilibrium constant. Further, an SCM can be utilized to predict the distribution of a substance between the sorbed and aqueous phase by assuming specific sorption mechanisms and the associated equilibrium constants.

The nonelectrostatic model (NEM) and constant capacitance model (CCM) are the two basic models that construct the bases of most surface complexation models for nuclide sorption. Both models are developed based on a set of assumptions common to all models. First, all mineral surfaces in an aquatic environment are assumed to contain functional groups, which are called surface sites, that have well defined properties. In essence, a sorbed ion is complexed, with inner-sphere or outer-sphere phases, by one or more ligands that are bound to the mineral structure. Second, for each type of surface site, a total concentration can be defined, according to specific experimental measurements, calculations or common assumptions. A recommended surface site density value of 2.311 sites/nm$^2$ was proposed by Davis and Kent (1990) for all minerals and the data is commonly utilized in the development of different SCMs. Third, the Gibbs free energy, $\Delta G_{ads}$, which involves two terms, can be defined for each sorption reaction. The $\Delta G_{ads}$ contains the effects of a chemical bond between the ion and the surface atoms ($\Delta G_{int}$) and an electrostatic effect that depends on the surface change ($\Delta G_{coul}$):

$$\Delta G_{ads} = \Delta G_{int} + \Delta G_{coul} \tag{8}$$

The intrinsic free energy, $\Delta G_{int}$, is specific to the surface and independent of the composition of sorption phase at a fixed ionic strength; while the coulombic free energy, $\Delta G_{coul}$, is variable with the distance from the surface, influenced by the diffuse double layer.

#### 2.2.4.3 The nonelectrostatic model (NEM)

The NEM model is the simplest surface complexation model. In this model, the variable electrostatic interaction, $\Delta G_{coul}$ shown in Equation (8), is ignored and the intrinsic constant alone is used to describe the sorption process, which means $\Delta G_{ads} = \Delta G_{int}$ and $K_{ads} = K_{int}$. This model is appropriate for the studying of sorption process without surface charge changes before and after sorption occurs. In the NEM, the determination of a sorption constant that describes a

surface complexation reaction simply reduces to an exercise in solving mass balance expressions.

#### 2.2.4.4 The constant capacitance model (CCM)

In the CCM, sorption is assumed to occur in a single surface plane that is a combination of the s-plane (for proton and hydroxide adsorption) and the is-plane (for metal and ligand adsorption). Thus, the inorganic surface hydroxyl groups are constrained to form only inner-sphere surface complexes with sorbed species. Outer-sphere surface complexes are not considered by the CCM. The CCM assumes a linear relation between surface charge, $\sigma$ and surface potential, $\psi$, which is given by

$$\sigma = \frac{C\ S\ a}{F}\psi \tag{9}$$

where X (F $m^{-2}$) is the capacity density, S ($m^2$ $g^{-1}$) is the specific surface area, a (g $L^{-1}$) is the suspension density of the solid and F (C $mol^{-1}$) is the Faraday constant.

In the CCM, the protonation and deprotonation reaction of the surface functional group can be determined by

$$\equiv SOH + H^+ \rightarrow \equiv SOH_2^+ \tag{10}$$

$$\equiv SOH \rightarrow \equiv SO^- + H^+ \tag{11}$$

The intrinsic conditional equilibrium constants expressing the protonation and deprotonation reactions are:

$$\mathrm{K}_+^{int} = \frac{[\equiv SOH_2^+]}{[\equiv SOH][H^+]}\exp(\frac{\Delta zF\psi}{RT}) \tag{12}$$

$$\mathrm{K}_-^{int} = \frac{[\equiv SO^-][H^+]}{[\equiv SOH]}\exp(\frac{\Delta zF\psi}{RT}) \tag{13}$$

The surface complexation reactions for specific ion adsorption have similar definitions as shown in Equations (10) to (13).

Both the NEM and CCM models can be used for Se sorption studies under specific experimental conditions. For example, Ervanne et al. (2016) modelled Se(IV) and Se(VI) sorption on kaolinite and illite in synthetic groundwaters with NEM successfully. The CCM was applied to Se(IV) sorption on various kinds of soils with different chemical properties (Goldberg et al., 2007). By optimizing one monodentate Se(IV) surface complexation constant and the surface protonation constant, the CCM was able to give satisfying fitting results of Se(IV) adsorption. Gabos et al. (2014) studied both Se(IV) and Se(VI) sorption on soil samples from São Paulo State, Brazil as a function of varying pH with CCM, and reasonable fitting results for both Se species were achieved.

#### 2.2.4.5 The 2SPNE SC/CE model

The 2 site protolysis non-electrostatic surface complexation and cation exchange (2SPNE SC/CE) sorption model, developed by Baeyens and Bradbury, has been used successfully to

describe quantitatively the uptake of radionuclides (e.g., Zn, Ni, Co, Eu and Sn) on montmorillonite (Baeyens and Bradbury, 1997; Bradbury and Baeyens, 1995, 2002; Michael H. Bradbury and Baeyens, 2005) and illite (Bradbury and Baeyens, 2009a, 2009b; M. H. Bradbury and Baeyens, 2005) as a function of pH, ionic strength and concentration of sorbates having oxidation states between II and VI. In the model, the cation exchange and surface complexation mechanisms are operating at the same time.

The model assumes two categories of sorption sites existing on the surface of a mineral. The first category of sorption site contains permanent negative charge arising from isomorphous substitution of lattice cations by cations of lower valance. The second category of sorption site is perceived as being surface hydroxyl groups ($\equiv SOH$) situated along the edges of the mineral's platelets. A detailed introduction of these two categories of sorption sites is presented in Section 2.2.1.

For the permanent negative charge sites (first category), charge neutrality is maintained by the presence of an excess of cations in solutions held electrostatically in close proximity around the surface. The electrostatically bound cation can undergo exchange with cations in solution, thus, cation exchange is assumed to be the dominant mechanism for the first category of sorption sites. In the general case, cation B with valance $z_B$ in the aqueous phase can exchange with cation A with valance $z_A$ which is bound to the mineral surface. The cation exchange reaction can be written as,

$$z_B \cdot A \equiv Mineral + z_A \cdot B \rightarrow z_A \cdot B \equiv Mineral + z_B \cdot A \tag{14}$$

The reaction equilibrium constant or selectivity coefficient, ${}^{B}_{A}K$, is defined to describe the reaction,

$${}^{B}_{A}K = \frac{N_B^{Z_A}}{N_A^{Z_B}} \cdot \frac{[A]^{Z_B}}{[B]^{Z_A}} \tag{15}$$

where [A] and [B] are the molar solution concentrations of cations A and B respectively, while $N_A$ and $N_B$ are equivalent fractional occupancies, defined as the equivalents of A or B sorbed per unit mass divided by the cation exchange capacity (CEC).

A selectivity coefficient can be derived from experimental data in the following way. The distribution ratio of cation B, ${}^{B}K_d$, can be written as,

$${}^{B}K_d = \frac{s_B}{[B]} = \frac{N_B \cdot CEC}{[B] \cdot Z_B} \tag{16}$$

At trace sorbate concentration, $N_A \sim 1$, Equation (15) can be rearranged to give,

$${}^{B}_{A}K = \frac{({}^{B}K_d)^{Z_A} \cdot {Z_B}^{Z_A} \cdot [A]^{Z_B}}{(CEC)^{Z_A}} \tag{17}$$

For the second category of sorption site, which is pH-dependent, strong ($\equiv S^{S}OH$) and weak ($\equiv S^{W}OH$) sorption site types were considered. The strong sorption sites are assumed to have a much smaller capacity but form considerably stronger complexes with sorbates and dominate

the sorption at trace concentrations. While at high concentrations, the effect of strong sorption sites is minimal and the weak sorption sites will dominate the sorption behaviour of ions.

A surface complexation reaction representing for example the sorption of M with valence $z_M$ on the strong sorption sites is written as,

$$\equiv S^SOH + M^{z_M} \rightarrow \equiv S^SOM^{z_M-1} + H^+ \quad (18)$$

The corresponding surface complexation constant, $K_M$, can be expressed as:

$$K_M = \frac{[\equiv S^SOM^{z_M-1}] \cdot \{H^+\}}{[\equiv S^SOH] \cdot \{M^{z_M}\}} \quad (19)$$

Outer sphere complexes of nuclides on different surface sites are not considered in the 2SPNE SC/CE model either. According to the modelling results, good agreement with the experimental data had been achieved over a wide range of conditions: pH, background electrolyte concentrations and sorbate concentration. Thus, on the basis of the currently available experimental evidence, it was not considered a necessity to introduce an additional parameter describing the formation of outer-sphere complexes.

In this thesis, a similar model was developed for Se(IV) sorption on biotite but with modified parameter acquisition and fitting procedures. A more detailed description of the model development is shown in Paper 2.

#### 2.2.4.6 Molecular modelling

Molecular modelling including the density functional theory (DFT) method has been widely used to obtain the sorption mechanisms at the molecular level. DFT is a method to determine the electronic structures and properties of materials. For example, DFT molecular modelling has been applied to estimate chemical reactions, solid material surface properties and surface sorption behaviour of various nuclides (Dash and Rath, 2020; Puhakka et al., 2020, 2019). Besides, the DFT method can be combined with spectroscopic characterization techniques such as X-ray absorption spectroscopy (XAS) including Extended X-ray Absorption Fine Structure (EXAFS) and X-ray Absorption Near-Edge Structure (XANES) to reveal the underlying phenomena and fundamentals of the sorption processes on mineral surfaces (Bower et al., 2019; Watts et al., 2019). For example, Watts et al. (2019) studied sorption of Cd(III) on gibbsite and kaolinite based on a combination of DFT molecular simulation and experimental data obtained from XAS. The DFT simulation results can reveal most bonding properties such as bond length/coordination numbers observed by XAS data. However, the author also pointed out that just DFT molecular modelling cannot capture all the true chemistry of the bidentate mononuclear interactions. A comparison of more molecular dynamics simulation methods could improve the simulation results.

In this thesis, molecular modelling was applied to provide sorption site information, such as sorption site types and site densities, for the development of SCM. In addition, molecular modelling was also performed to examine, at the molecular level, the complexation reactions assumed in the SCM, thus, providing more theoretical support of the SCM developed.

## 2.3 Diffusion Process

In order to understand the spatial and temporal variability of a radionuclide migrating through bedrock, it is essential to have an overall perception of the chemical and physical processes happening in the flowing fracture water and in the matrix pore water. The radionuclides in the fracture water are retarded compared to the velocity of water along a flow path by chemical processes like cation exchange reactions and surface complexation reactions on the minerals of the bedrock. Furthermore, physical processes, like flow, diffusion and dispersion, will cause mixing and smoothen concentration changes. Because the pore openings of bedrock are in micrometre and nanometre scale which caused that the pore water is stagnant, the main process for retarding the nuclides' transport compared to water movement is matrix diffusion.

### 2.3.1 Definitions and Fick's laws

Diffusion is defined as the net movement of ions and molecules from a region of higher concentration (or high chemical potential) to a region of lower concentration (or low chemical potential) caused by the random Brownian movement of atoms and molecules. The movement of molecules by diffusion is described by Fick's laws (Crank, 1979). Fick's first law relates the flux of a chemical to the concentration gradient:

$$F = -D\frac{\partial c}{\partial x} \tag{20}$$

where F is the flux (mol/s/m$^2$), D the diffusion coefficient (m$^2$/s), and c the concentration (mol/m$^3$).

Fick's second law describes the rate at which concentration is changing at any given point in space. In one dimension, Fick's second law can be written as,

$$\frac{\partial c}{\partial t} = D\frac{\partial^2 c}{\partial x^2} \tag{21}$$

where t is the time of diffusion (s).

Compared to diffusion in "free" water, nuclides diffusion through a water saturated porous rock matrix is a complex process where the geometrics of porosity, tortuosity and constrictivity has to be taken into account. The effective diffusion coefficient, $D_e$, was proposed to account for the entire pore space. In a saturated porous medium, De is related to the free water diffusion coefficient and defined as,

$$D_e = \frac{D_w \varepsilon_t \delta}{\tau^2} \tag{22}$$

where $D_w$ is the diffusion coefficient in "free" water; $\varepsilon_t$ is the porosity available for the transport; $\delta$ is the constrictivity and $\tau$ is the tortuosity.

The effective diffusion coefficient can also be related to formation factor, $F_f$, which is the ratio of the specific electrical resistance of sediment with a solution and the specific resistance of the free solution. The formation factor is defined by the geometry of the porous system and dependent on the porosity, constrictivity and tortuosity,

$$F_f = \frac{\varepsilon_t \delta}{\tau^2} \tag{23}$$

Thus, the effective diffusion coefficient can be expressed as,

$$D_e = D_w \cdot F_f \tag{24}$$

### 2.3.2 Measurements of diffusion parameters

The diffusion of nuclides migrating through the bedrocks can be studied experimentally by various techniques. The block scale diffusion experiment (García-Gutiérrez et al., 2006; Ikonen et al., 2016) and through-diffusion experiment (Kuva et al., 2015; Puukko, 2014; Tachi et al., 2015) are the two traditional techniques for diffusion studies in crystalline rocks. The common problem with these techniques is that the experiments are quite time consuming and normally months or even years is required before enough samples can be collected at the outlet position. The reason is that the permeability of the rock matrix is very small due to the very low porosity of the bedrock samples. Normally, the porosity of a crystalline bedrock rock sample is in the order of $10^{-3}$ and the apertures of its micropores are in the order of micrometres to nanometres (Möri et al., 2003). Thus, the pore water in the rock matrix can be considered as stagnant and the main process for retarding the nuclides' transport compared to water movement is matrix diffusion by Brownian motion. As a result, long time will be used for studied nuclides migrating from the source position to the sampling position.

New techniques have been developed to reduce the experimental time to a laboratory acceptable level. For example, hydraulic pressure can be used to accelerate the transport of the studied ions in rock matrix. However, because of the low permeability of the rock sample, high hydraulic pressure is often required to accelerate the movement of tracer ions. Gas phase through diffusion experiments using He atom as a tracer has been developed at the University of Jyväskylä some years ago (Kuva et al., 2016, 2015). The method can reduce the experimental time by about 11,000 times based on the fact that the diffusion coefficient of He in nitrogen is about 11,600 times larger than that of He in water. However, water-based experiments can provide more realistic results because in the gas phase experiments, the chemical effects and other water-phase related interactions (e.g. solute-mineral surface interactions) are ignored. The gas phase through diffusion experiments are more suitable for providing bulk diffusion coefficients for safety case calculations from pure physical point of view. Compared with the above-mentioned techniques, the electromigration method is more advantageous. The electromigration device, designed by Löfgren and André, can be shown schematically in Figure 11 (André et al., 2009; Löfgren and Neretnieks, 2006). An electric field is applied to accelerate the migration of charged ions in pore water inside the studied rock sample which is placed between two chambers, one holding an electrolyte with high tracer concentration and one holding an electrolyte initially free of the tracer. The speed of the studied ion can be controlled by applying a proper potential over the intact rock sample and a small electrical field is efficient enough to accelerate the migration of charged ions in pore water inside a low-permeability granitic rock core (Maes et al., 1999; Mitchell and Soga, 2005). As a result, the experimental time could be reduced significantly to several days or weeks.

The electromigration technique has been used for studies such as $D_e$, $K_d$, CEC and $F_f$ in crystalline bedrocks (André et al., 2009; André et al., 2009; Puukko et al., 2018) and clay soils (Beauwens et al., 2005; Maes et al., 2002, 1999). However, some critical flaws still exist in the current design of the device and results analysis methods as we pointed out in Paper 4. In this thesis, we modified the electromigration device based on the current problem. The new device was tested by determining the $D_e$ and $F_f$ values of Se(IV) species migrating through an intact rock sample from the Äspö underground laboratory (Paper 4). In addition, a new model called advection-dispersion model was developed for better analysis of the electromigration experimental results (Paper 5).

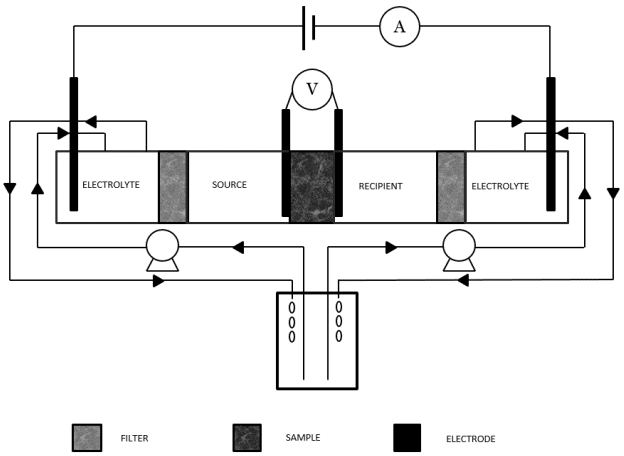


*Figure 11. Schematic setup for electromigration experiments modified from Löfgren and Neretnieks (2006).*

### 2.3.3 Modelling of diffusion in the rock matrix

Normally, both diffusion and sorption should be taken into account when we talk about modelling of diffusion because of the dramatic retardation effect for sorbing nuclides. To assure strict mathematical description, four assumptions are made based on the geometry and hydraulic properties of the system. First, the aperture is assumed to be much smaller than the length of the fracture; second, transverse diffusion and dispersion within the fracture always ensure complete mixing across its aperture; third, transport within the matrix is dominated by molecular diffusion owing to the low permeability of porous rock; fourth, transport along the fracture is much faster than that within the matrix. The first two assumptions ensure that it is reasonable to describe the solute transport along the fracture in one dimension and the remaining two assumptions indicate that the direction of tracer migration in the matrix is perpendicular to the fracture coordinate x. Based on these assumptions, the commonly used advection-dispersion model can be formulated in mathematical term, neglecting hydrodynamic dispersion, by the following differential mass balance.

Diffusion in the rock is given by,

$$\frac{\partial c_p}{\partial t} = \frac{D_e}{\varepsilon_p + K_d \rho} \frac{\partial^2 c_p}{\partial z^2} - \lambda c_p = D_a \frac{\partial^2 c_p}{\partial z^2} - \lambda c_p \tag{25}$$

For flow and solution from the water in the fissure we have

$$\frac{\partial c_f}{\partial t} + u \frac{\partial c_f}{\partial x} = \frac{D_e}{b} \cdot \frac{\partial c_p}{\partial z}\bigg|_{z=0} - \lambda c_f \tag{26}$$

where $c_p$ is the concentration in water in pores; $c_f$ the concentration in water in fissures; $x$ the distance along a fissure; $z$ the distance into the rock from fissure surface; $b$ the half-width of fissure; $u$ the water velocity in fissure; $\rho$ the rock density; $\lambda$ the decay time constant; $D_a$ the apparent diffusivity.

In Equation (26), the water flows in the x direction while the diffusion happened in the z direction into the rock matrix. The Equations (25) and (26) are the basic equations upon which most solute transport models are based. The models differ mostly in how the equations are implemented in different conceptualisations of the rock mass. For example, for a system which is initially free of nuclide and where the nuclide concentration suddenly is increased to $C_0$ at the inlet of the fissure (x=0), the initial and boundary conditions are defined as,

Initial condition

$$c_p = c_f = 0 \qquad t < t_0 \quad all\ x\ and\ z \tag{27}$$

Boundary condition 1

$$c_p = c_f = 0 \qquad when\ t > 0 \quad for \quad z \to \infty \tag{28}$$

Boundary condition 2

$$\begin{gathered} c_f = 0 \qquad for \quad t < t_0 \quad at \quad x = 0 \\ c_f = c_0 \cdot e^{-\lambda t} \qquad for \quad t_0 \le t \le t_0 + \Delta t \quad at \quad x = 0 \\ c_f = 0 \qquad for \quad t > t_0 + \Delta t \quad at \quad x = 0 \end{gathered} \tag{29}$$

For $\lambda > 0$ the solution is obtained by the Laplace transformation method (For a stable species ($\lambda = 0$), for $t_0 = 0$ and $\Delta t \to \infty$, the solution is available in the literature (Carslaw and Jaeger, 1959),

$$\frac{c_p}{c_0} = e^{-\lambda t}\left\{erfc\left[\frac{G}{\left(t - (t_w + t_0)\right)^{1/2}}\right] - erfc\left[\frac{G}{\left(t - (t_w + t_0 + \Delta t)\right)^{1/2}}\right]\right\} \tag{30}$$

where

$$G = \{[D_e + \frac{1}{2}\frac{u(2b)z}{x}]/2b(D_a)^{\frac{1}{2}}\} \cdot t_w \quad (31)$$

The solution applied only for $t > t_w + t_0$ for the first erfc expression, which otherwise is 0, and $t > t_w + t_0 + \Delta t$ for the second erfc expression, which otherwise is 0.

For the fluid in the fissures of the rock, $c_f/c_0$ is obtained by setting z = 0. Boundary condition 2 (Equation (29)) is used here because it simulates a constant leach rate of a body containing a decaying nuclide. This is one of the important cases to study. Equations (30) and (31) apply only when the penetration thickness is considerably smaller than the fissure spacing.

A detailed introduction of the basics of the model is available in Neretnieks (1980) and Liu et al. (2006). The analysis of the analytical solution to the governing equations (Equations (25) and (26)) can be found in Tang et al. (1981) and Sudicky and Frind (1982). In this thesis, we have developed an advection-dispersion model based on Equations (25) and (26) for accurate analysis of the electromigration results. In the model development, both convection and dispersion were involved as a result of the application of an electric field to accelerate the movement of studied nuclides.

# 3 Experimental

## 3.1 Characterization of rock samples and groundwaters

The rock samples for sorption experiments, Grimsel granodiorite, was supplied by the underground research laboratory in Grimsel test site where a long-term in-situ diffusion experiments were conducted (from 2013 to 2017). The results from this work were meant to supply laboratory scale data for effective evaluation of both the laboratory and in-situ experimental results (Muuri et al., 2018, 2016; Soler et al., 2015). Granodiorite is a medium grained and slightly foliated granite. The composition of its main mineral was analyzed by X-ray Powder Diffraction (XRD) method, and the results show that plagioclase (40%), potassium feldspar (25%), quartz (20%) and biotite (10%) are the main mineral composition of Grimsel granodiorite. The remaining minerals, chlorite, green amphibole (hornblende), muscovite, epidote etc., are less than 5%. The porosity of Grimsel granodiorite varies from 0.5% to 1.5% (Kelokaski et al., 2006) and permeability is $(1.3\pm0.3) \times 10^{-7}$ $m^2$ (Ikonen et al., 2016).

The pure minerals for sorption experiments, plagioclase, biotite and K-feldspar, were provided by the Geological Survey of Finland. Quartz was bought from UKGE which is a geological and expedition supplier in the UK. All the pure minerals as well as the Grimsel granodiorite were crushed by milling and the part with particle size between 0.071 mm and 0.3 mm were sieved out for later analysis and experiments. Mineral composition analysis of the rock and mineral samples was performed by XRD method at the Geological Survey of Finland. Specific surface area (SSA) measurement was determined at Chalmers University with Kr gas adsorption Brunauer-Emmett-Teller model (Kr-BET) method using gas adsorption analyzing instrument. Cation exchange capacities (CEC) of all the rock and mineral samples were measured with ammonium acetate method (Dohrmann, 2006).

The porosity of intact the rock sample was measured by a water weight difference method as shown in Ohlsson (2000) and Löfgren (2005). The rock sample was first dried in a vacuum drier for 3 weeks and the weight of the totally dried sample was recorded. Then the sample was fully saturated with 0.2 M NaCl solution using the method shown in Löfgren (2005). After achieving fully saturation, the weight of the rock sample was followed as a function of time until the surface of the rock sample was fully dried. The surface dry weight was obtained from the intersection between the two lines drawn from the drying curve, as shown in Figure 20. The porosity of the rock sample can be calculated by the difference of the weight of rock sample with dried surface and the weight of totally dried rock sample as well as the density of the electrolyte.

A Grimsel groundwater simulant (GGWS) was prepared as background electrolyte in the batch sorption experiments. The elemental composition of the groundwater simulant was presented in Table 1.

*Table 1. The elemental composition of GGWS and the compostion of fracture water in Grimsel test site.*

| | pH | $Na^+$ | $K^+$ | $Ca^{2+}$ | $Mg^{2+}$ | $HCO_3^-$ | $Cl^-$ | $SO_4^{2-}$ | $Br^-$ | $F^-$ | $Si^{**}$ |
|---|---|---|---|---|---|---|---|---|---|---|---|
| Grimsel water (mg/L) | 9.7 | 15.87 | 0.195 | 5.60 | 0.015 | 27.45 | 5.67 | 5.86 | 0.03 | 6.84 | 7.00 |
| GGWS (mg/L) | 9.5* | 25.53 | 0.195 | 5.60 | --- | 27.45 | 5.67 | 5.76 | --- | 6.84 | 7.00 |

## 3.2 Sorption studies

### 3.2.1 Titration and sorption experiments

The purpose of the sorption studies is to make a multi-site surface complexation model that can be used to predict the sorption of Se(IV) species on the bedrock of a nuclear waste repository (Grimsel granodiorite in this work) under a wide range of groundwater conditions. Three sets of experimental data were required for deducing a multi-site surface complexation model, as shown schematically in Figure 12. Each set of experimental data will provide different parameters necessary for the sorption model development.

#### 3.2.1.1 Titration measurements

The titration results give information about the amount of net-consumed $H^+$ or $OH^-$ by different sorption sites in the protolysis reactions (Equations (2) and (3)). Thus we can deduce the mineral surface site capacities and intrinsic surface protonation and deprotonation constants ($K_{int}(+)$, $K_{int}(-)$) for amphoteric ≡SOH type surface sites. The titration experiments were carried out in an inert $N_2$ atmosphere glovebox with the concentration of $CO_2$ being < 10 ppm and the concentration of $O_2$ being < 1 ppm. The purpose was to minimise the influence of $CO_2$ on the pH measurements and mimic the redox conditions of underground water. Titration was carried out in a batch-wise manner to ensure the achievement of equilibrium during the titration process. First, K-converted biotite was equilibrated with 0.01 M $KClO_4$ solution for 3 days. Then, standard acid or base was added to get a series of initial pH conditions from 3 to 11. The whole system was left for equilibrium for another 3 days during which time additional acid or base was added to compensate for the pH changes because of mineral dissolution and surface reactions. After titration, the cation concentrations (Na, K, Ca, Mg, Al) in the solution phase were checked, at the same time the solution phase was back-titrated to initial pH 7 to calibrate the mineral dissolution during the titration process. The titration results were also further calibrated with cation exchange and proton exchange effects by determining the selective coefficients of cation/proton exchange reactions between corresponding cations and $K^+$ ions on the biotite surface.

#### 3.2.1.2 Sorption edge measurements

The sorption edge studies provide the information of Se(IV) sorption behaviours as a function of pH at fixed ionic strength in a trace concentration. According to the assumptions, strong sorption sites ($\equiv S^S OH$) will dominate the Se(IV) species behaviours in the low concentration

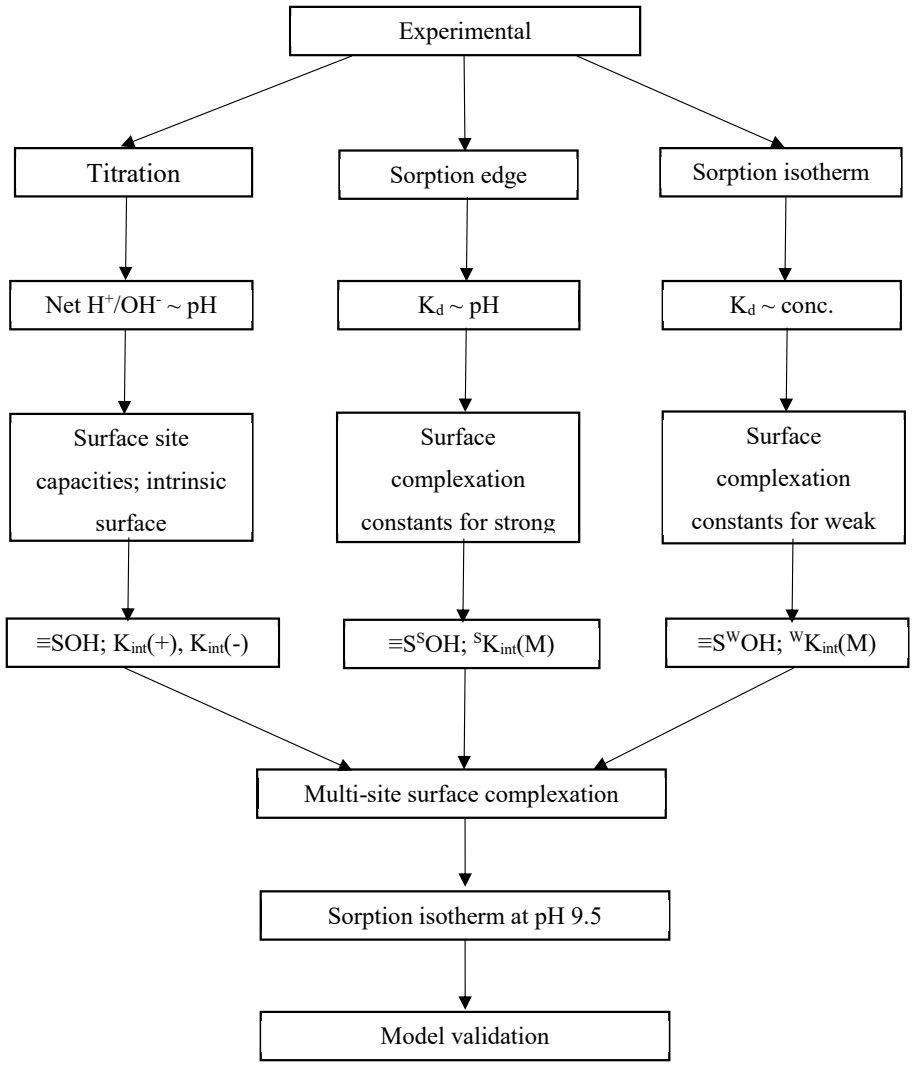


*Figure 12. Schematic figure of the experimental procedures of surface complexation modelling.*

area (< $10^{-7}$ M) while the weak sorption sites (≡$S^{W}OH$) will dominate the Se(IV) species behaviours in the high concentration area (>$10^{-6}$ M). Thus, we can deduce the surface complexation reactions that happened on the strong sorption sites and the corresponding reactions constants. Sorption edge measurements were carried out with a trace amount of radioactive Se-75 in a glovebox. First, K-converted biotite was equilibrated with 0.01 M $KClO_4$ for 3 days. Then standard acid and base were added together with a proper amount of Se-75 and a series of samples with pH from 3 to 11 and Se concentration at 10-9 M were made. The samples were shaken to achieve equilibrium for 7 days during which time the pH was adjusted by adding acid and base. After sorption experiments, the amount of Se-75 in the solution phase was checked by the Hidex-AMG gamma counter and the $K_d$ values were calculated by the equation,

$$K_d = \frac{C_0 - C_{aq}}{C_{aq}} \times \frac{V}{m} \quad (32)$$

where $C_0$ is the initial concentration of Se in the solution; $C_{aq}$ is the final concentration of Se after sorption equilibration; V is the volume of the solution and m is the mass of the solid phase.
Sorption isotherm measurements

The sorption isotherm data shows the sorption of Se(IV) ions on mineral surfaces on both high and low concentrations areas at a fixed pH and temperature condition. Combined with the strong sorption site information provided by sorption edge results, we can deduce the surface complexation reactions and the corresponding reaction constants for weak sorption sites. The sorption isotherm measurements were carried out at fixed pH conditions (~7.8) with batch sorption methods. After equilibrating the biotite samples and 0.01 M $KClO_4$ solution, a series of samples with the Se concentrations from $10^{-10}$ M to $10^{-3}$ M were made by adding proper amount of stable Se and radioactive Se-75. Then the mixtures were shaken for another two weeks to achieve fully sorption equilibration. The $K_d$ values of Se species in the samples were calculated by Equation (32) shown above.

### 3.2.2 Surface complexation modelling (SCM) development

The main purpose of the modelling processes is to find a set of parameters that can fit all the experimental data. If a set of parameters can be reached, it is believed that it can reasonably reflect the real properties of Se(IV) sorption processes on biotite.

The modelling procedure was carried out in an iterative way (Figure 13). The set of parameters fitted in one step will be fixed in the subsequent steps. If a "break down" appears, the fitting process will go back to some earlier steps for modification of the modelling parameters until a set of parameters can fit all the experimental data.

The titration results should be fitted first since it provides the most basic parameters (protonation/deprotonation constants, $K_{int}(+)$, $K_{int}(-)$) for further sorption edge and sorption isotherm simulations. In this work, three types of sorption sites were considered; one type of strong sorption sites ($\equiv S^SOH$) and two types of weak sorption sites ($\equiv S^{W1}OH$ and $\equiv S^{W2}OH$). The reason why we assumed two types of weak sorption sites existing on biotite surfaces is based on the fact of molecular modelling results (Section 3.2.3). The modelling results show that one type of the weak sorption site exists on the basal surface of biotite with site density of 3.2 sites/nm$^2$ while the other one on the edge surface of biotite with site density of 1.4 sites/nm$^2$.

The sorption edge and sorption isotherm data are considered to give information of reaction constants between different Se(IV) species and the three types of sorption sites. For all the fitting and optimization processes, a code that coupled PHREEQC and Python was developed. PHREEQC is a computer program that can perform calculations of a wide variety of geochemical processes, such as speciation, surface complexation, ion exchange, 1-D diffusion etc. Python is a high-level computer programming language which was used in this work to control the modelling flow and perform optimization of the modelling results by "fmin" function in the Scipy package. The "fmin" function can find the optimized modelling results by minimizing the squares of the difference between experimental and modelling simulated data.

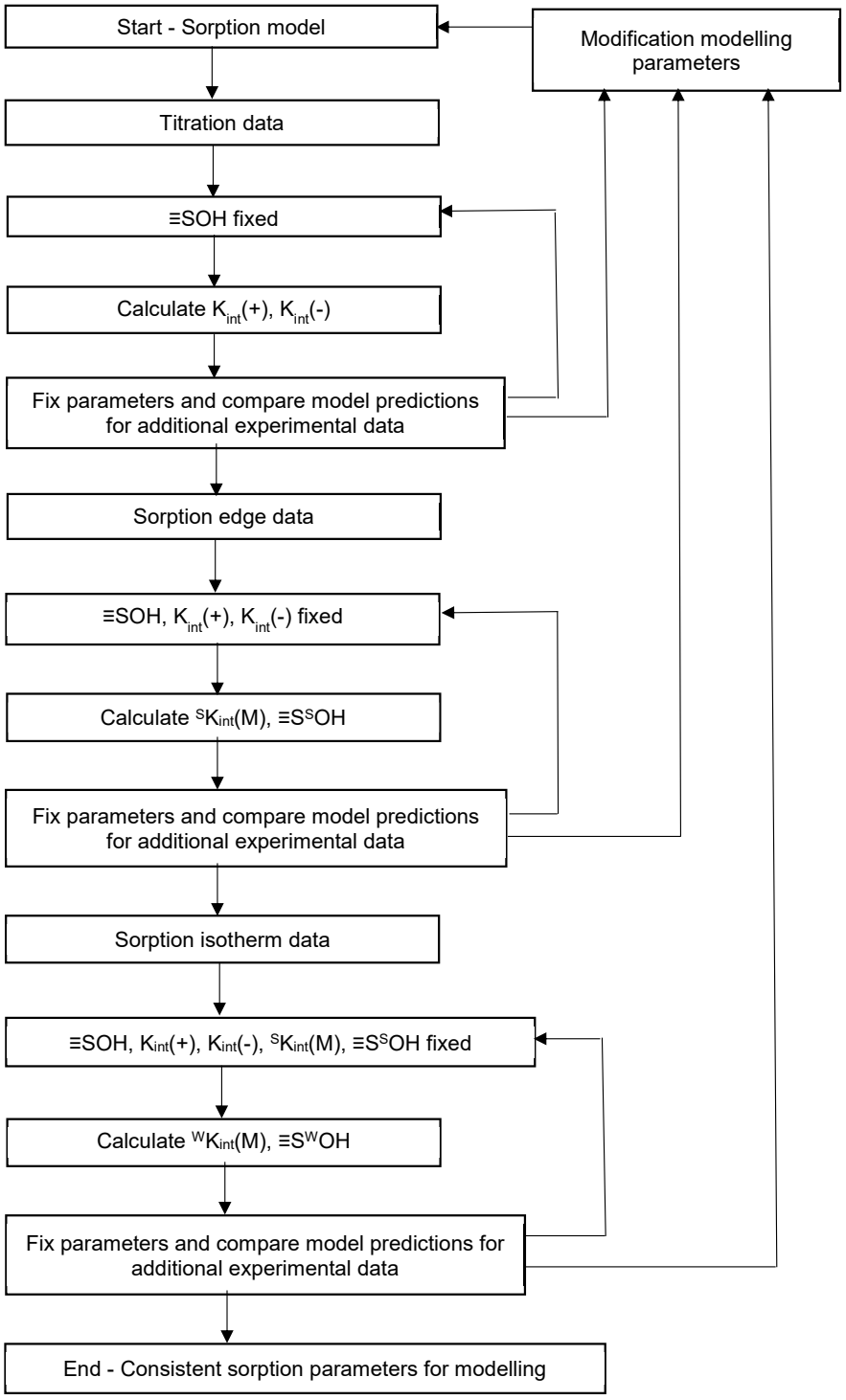


*Figure 13. Schematic figure of the iterative procedure of multi-site surface complexation modelling.*

### 3.2.3 Molecular modelling with DFT methods

Molecular modelling was performed to investigate the crystalline surface structures and sorption sites on biotite surfaces, give support parameters for the development of SCM, and examine the complexation reactions that happened on biotite surface. Thus, molecular modelling can not only give support parameters such as sorption site types and site densities for SCM, but can also provide theoretical support for the assumed reactions in the SCM. The calculations were performed with the CASTEP (CAmbridge Serial Total Energy Package by Clark et al. (2009)) code implemented into Materials Studio version 8.0. The modelling is based on solving total electronic energy and overall electronic density distribution in order to define energetically stable structures for minerals and sorbing species (Leach, 2001). The exchange-correlation was described with generalized gradient approximation GGA-PBE. As a compromise between the accuracy and computational time of calculations, the ultrasoft pseudopotentials were used for each element. The potentials used were Al_00PBE.usp for aluminium, H_00PBE.usp for hydrogen, O_soft00.usp for oxygen, Se_00.usp for selenium, and Si_soft00.usp for silicon. The kinetic cut-off energy for a plane wave expansion of the wave function was 230 eV. The cut-off values correspond to fine quality for all the atoms, except for oxygen and selenium.

## 3.3 Diffusion studies

### 3.3.1 Modification of the electromigration device

The design of the electromigration device by Löfgren and André is shown in Figure 11. In our work, we performed several modifications based on their design by considering some critical flaws existing in it. The modified device has the functions of voltage-self-controlling, continuous-current-recording and solution-pH-stabilization, which are lacking in Löfgren and André's design.

First, we introduced a potentiostat (Figure 14, left) to automatically control the voltage over the rock sample precisely (±0.01 V) within the whole experimental period. The precise controlling of the voltage was achieved by applying the four-electrode function of the potentiostat (Figure 14, right). The four-electrode function enables the potentiostat to adjust automatically the whole voltage applied over the electromigration device to give a constant potential over the rock sample according to the change of the resistance of pore solution. Thus, the stability of the device can be improved significantly and long-term running of the device becomes possible.

Second, the current flowing through the rock sample can be recorded automatically and continuously by the potentiostat. The variation of the current gives information on the movement and distribution of ions inside the rock sample under an electric field, thus, it is an important factor to be considered when analyzing the experimental results and future reactive transport modelling.

The controlling of pH of background electrolyte during the running of the electromigration device is crucial. If the pH is changed, firstly, some ionic tracers, such as $SeO_3^{2-}$, may become protonated and deprotonated. This will change the overall charge of the selenite ions. Secondly, the minerals may become altered and may dissolve significantly if a rock sample is subjected

to large pH changes, which may affect the transport properties of the rock. Thirdly, the efficiency of transferring current from the electrode surfaces to the electrolytes will change if pH changes are allowed in the electrolytes.

However, electrolysis of background electrolytes occurs at the anode and cathode during the running of the electromigration experiments,

$$\text{Anode: } 2H_2O - 4e^- \rightarrow 4H^+ + O_2 \quad (33)$$

$$\text{Cathode: } 2H_2O + 2e^- \rightarrow 2OH^- + H_2 \quad (34)$$

As a result of electrolysis, the pH will change with the running of the device, though the anode and cathode are separated in different chambers to reduce the effect of electrolysis. In our experiment, we buffered the background electrolyte by adding proper amount of $NaHCO_3$ to the NaCl solution which was commonly used as background electrolyte in previous studies. The addition of $NaHCO_3$ has two functions. Firstly, $NaHCO_3$ simulates the pH level of real groundwater while the concentration of NaCl simulates the ionic strength. Secondly, $HCO_3^-$ ~ $CO_3^{2-}$ in the solution is a pH-buffer pair. Even if some amount of $H^+$ or $OH^-$ migrate into the tracer chambers from the electrode chamber, they would not cause significant changes in the pH value because of the buffer effect of $HCO_3^-$ ~ $CO_3^{2-}$ pair.


*Figure 14. Left: the potentiostat introduced to the electromigration device system to keep a constant voltage over the rock sample and record the current. Right: the connection of the four-electrode system.*

### 3.3.2 Development of data analysis approach

The traditional approach of data analysis for electromigration experimental results, the ideal plug-flow model, involves many unrealistic assumptions and therefore, it had better be used to make a rough estimate of the diffusion and sorption properties of the solute species. Since it commonly gives large uncertainties in parameter identification, one may use the results to define the lower and upper bounds of the corresponding parameters for a better evaluation by an advanced model.

In this work, an advection-dispersion model was developed with the purpose to interpret the experimental results with more confidence. It accounts for the most important mechanisms governing the movement of the tracer ions, i.e. electromigration, electroosmosis and dispersion. By comparison, the ideal plug-flow model just considered electromigration effect in the model

development. The advection-dispersion model was formulated on the basis of the equation of continuity describing the mass balance of the tracer ions over a rock sample perpendicular to the direction of mass transport. An analytical solution in the Laplace domain was derived and then the inverse Laplace transform of the solution can be obtained by use of e.g. $D_e$ Hoog algorithm (de Hoog et al., 1982) to numerically transform back to the time domain. The solution in the time domain gives the tracer concentration at the recipient chamber, $c_R$, which was measured by the updated electromigration device. By fitting of the numerical solution, $c_R$, to the experimentally determined data, the parameters like effective diffusion coefficient, $D_e$, and retardation factor, R, can be evaluated with suitable lower and upper bounds.

### 3.3.3 Electromigration measurements

The modified electromigration device was tested by running with three kinds of tracers: quinoxaline for electroosmosis measurements, NaI for $I^-$ measurements and $Na_2SeO_3$ for Se(IV) species measurements. The background electrolyte used was 0.2 M NaCl + 0.002 M $NaHCO_3$ (pH was adjusted to be ~ 8.5 before using). The potential difference over the rock samples was set to be 2V and 4V which were controlled to be constant by the potentiostat as discussed above.

Before running with the tracers, the electromigration device was stabilised by running with background electrolyte for 3 days. After stabilisation, proper amount of tracers were added into the source chamber and the final concentration of the tracers was 0.1 M. Same amount of NaCl was added to the recipient chamber to balance the ionic strength. The initial conditions of the experiments are summarised in Table 2. During the running of the electromigration experiments, 2 mL samples were taken from the recipient chamber from time to time to follow the concentration change of the tracers. At the same time, same amount of background electrolytes was added into the recipient chamber to keep the hydraulic pressure and the volume of solutions to be constant between the source and recipient chambers.

*Table 2. Summarise of the electromigration device parameters and initial experimental conditions. The tracers were tested separately with the electromigration device.*

| Experimental set-up | | |
|---|---|---|
| Source/Recipient chamber volume | Diameter of the source/recipient chambers | Working temperature |
| 152 mL | 5 cm | ~25 ℃ |
| Rock sample | | |
| Length | Diameter of the rock sample | Porosity |
| 1.12 cm | 5 cm | 0.7% |
| Background electrolyte | | |
| pH | NaCl concentration | $NaHCO_3$ concentration |
| ~8.5 | 0.2 M | 0.002 M |
| Tracers and working conditions | | |

| | | |
|---|---|---|
| Quinoxaline/NaI/$Na_2SeO_3$ in source chamber | Quinoxaline/NaI/$Na_2SeO_3$ in recipient chamber | Voltage over the rock sample |
| 0.1 M | 0 | 2V and 4V |

The experimental results were analysed by both the traditional ideal plug-flow model and the advection-dispersion model developed in this thesis. For the analysis with the ideal plug-flow model, a linear regression line was drawn with the last several data points where a pseudo steady state seems to be established. The intercept of the regression line with the time axis is an estimation of the breakthrough time ($t_{br}$) of the tracer ion and the slope of the linear regression line ($\frac{d_c}{d_t}$) is describes the concentration change of it in the recipient chamber under the steady-state condition. The effective diffusivity, $D_e$, of tracer ion in the rock sample can be determined using Equation (35).

$$D_e = \frac{V \cdot \kappa \cdot T \cdot \frac{d_c}{d_t}}{A \cdot c_t \cdot e \cdot z \cdot \frac{d_\varphi}{d_x}} \tag{35}$$

The formation factor, $F_f$, was then determined with Equation (24) in the ideal plug-flow model.

The advection-dispersion model, instead, analyses the whole breakthrough curve by fitting with Equation (66) shown in this thesis. The $D_e$ and $F_f$ values can be obtained by the best fitting of the modelling results to the experimental data points.

The parameter identification results ($D_e$ and $F_f$) with the traditional ideal plug-flow model and the newly developed advection-dispersion model were compared. The migration behaviours of iodide, which was considered to be a non-sorbing ion, and Se(IV) ions, which are slightly-sorbing ions, were also compared in this thesis.

# 4 Results and Discussion

## 4.1 Results of sorption studies

### 4.1.1 Characterization results of rock and mineral samples

The mineral characterization (XRD) of Grimsel granodiorite shows that plagioclase, K-feldspar, quartz and biotite are the main mineral compositions of it (Table 3). The purities of the main minerals used for batch sorption experiments are also listed in Table 3. The SSA results show that biotite has the largest SSA value which is due to the layer sheet structure of it, providing roughness to the surface and large area of inner surface. Plagioclase has the largest CEC value; while the CEC value of biotite is the second largest. Considering both SSA and CEC values among all the rock and mineral samples, we can predict that biotite may play an important role in the sorption of radionuclides such as Se-75. This result has been confirmed in the work of Yang et al. (2018), in which it shows, by the studies with EPMA (Electron Probe Micro-Analyzer) analysis, that biotite can be representative of the Se(IV) sorption in complex mineral assemblages such as granite and biotite contents are critically important to evaluate Se(IV) transport in granite.

*Table 3. Characterization results (XRD, SSA, CEC) of Grimsel granodiorite and its main minerals.*

| Rock/mineral | XRD<br>Main minerals in samples as percentages | SSA ($m^2/g$) | CEC (meq/Kg) |
|---|---|---|---|
| Grimsel granodiorite | 40% plagioclase, 25% K-feldspar, 20% quartz, 10% biotite and 5% chlorite | 0.1268 | 3.32 |
| Plagioclase | 75% plagioclase; 5% biotite, 5% K-feldspar, 5% amphibole; chlorite, quartz, magnetite, ilmenite altogether < 10% | 0.1150 | 22.69 |
| Biotite | 100% | 1.0323 | 12.64 |
| Quartz | 100% | 0.0486 | 0.01 |
| K-feldspar | 90% K feldspar, 8% plagioclase and 2% quartz | 0.1084 | 1.68 |

### 4.1.2 Selenium speciation in the sorption experiments

The long time scale of sorption and diffusion experiments makes it possible that selenite ($SeO_3^{2-}$) ions added into the experimental device could be oxidized to selenate ($SeO_4^{2-}$), according to the Eh-pH diagram of Se species (Figure 4), though the transformation between Se(IV) and Se(VI) ions is believed to be slow and kinetically hindered because it involves the transfer of multiple electrons and oxygen atoms, in this thesis,

HPLC-ICP-MS technique was applied to separate the Se(IV) and Se(VI) species after sorption isotherm experiments which took up to one month period; and the amount of Se species in both valance states were measured with ICP-MS. The results (Figure 15, left) showed no sign of

selenate and it confirmed that all Se(IV) ions remained in their +IV oxidation state during the period of sorption experiments.

The aqueous speciation of Se(IV) ($SeO_3^{2-}$, $HSeO3^-$, $H_2SeO_3$) was calculated as a function of pH from 3 to 11, based on the speciation data from Ervanne et al. (2016) and the calculated speciation distributions are shown in *Figure 15*, right. $HSeO3^-$ is the dominant species when pH is below 8.5, while for pH above 8.5, the main species is $SeO_3^{2-}$. For the pH conditions of natural groundwater which is slightly basic, both $SeO_3^{2-}$ and $HSeO3^-$ can exist in groundwater.

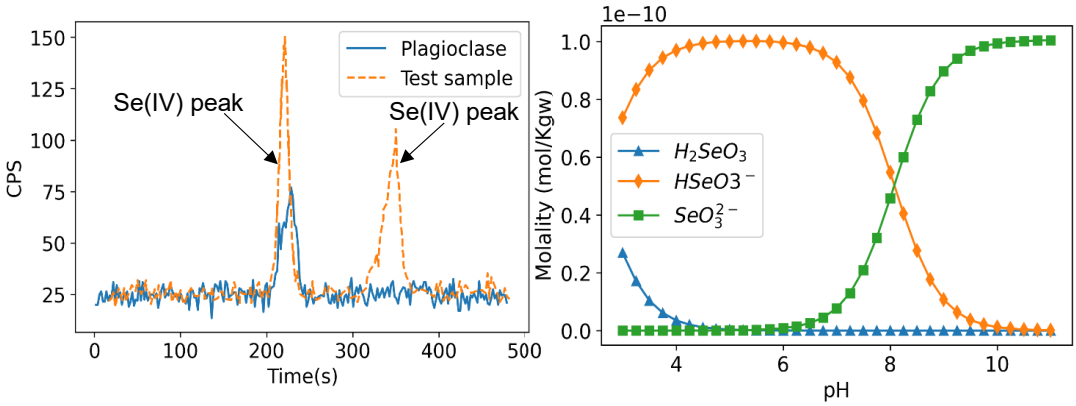


*Figure 15. Left: HPLC-ICP-MS results of selenium species after one month stabilization time with crushed plagioclase and a reference water sample containing only $Na_2SeO_4$ at $10^{-7}$ M concentration level; Right: the result of selenium speciation as a function of pH from 3 to 11 calculated with PHREEQC.*

### 4.1.3 Titration results

One of the most difficult problems when performing titration experiments with minerals is mineral dissolution. The ignorance of mineral dissolution will cause two high $H^+$ and $OH^-$ consumption in the extreme pH areas (pH < 5 or pH > 10). Figure 16a shows clearly that the consumed $H^+$ and $OH^-$ rises sharply at extreme pH areas, indicating severe dissolution of biotite.

In order to overcome the problem of mineral dissolution, we used a batch titration coupled with backtitration method in this thesis. In this method, the titration was performed in batch-wise manner, instead of a continuous manner, and the supernatants from forward titration samples were back-titrated to a common endpoint. The quantities of acid or base consumed in the backtitration are subtracted from the quantities of base or acid consumed in the forward titration.

In the case of acid titration, biotite the composition of which is characterized as $(KMg_{1.76}Fe_{0.7}Ti_{0.54})(Al_{1.08}Si_{2.92}O_{10})(OH_{0.44}F_{0.56}O)$, will dissolve in the acidic solution in the forward titration process,

$$(KMg_{1.76}Fe_{0.7}Ti_{0.54})(Al_{1.08}Si_{2.92}O_{10})(OH_{0.44}F_{0.56}O) + 1.32H_2O + 8.6H^+ \Leftrightarrow K^+ + 1.76Mg^{2+} + 0.7Fe^{2+} + 0.54TiO_2 + 1.08Al^{3+} + 2.92H_4SiO_4 + 0.56F^- \quad (36)$$

and 8.6 mol of $H^+$ are consumed by dissolution reaction of 1 mol of biotite. While in the backtitration process, by titrating with base to the neutral conditions, the following species are formed,

$$\begin{aligned} &K^+ \Longrightarrow K^+ \\ &1.76Mg^{2+} \Longrightarrow 1.76Mg^{2+} \\ &0.7Fe^{2+} + 1.4OH^- \Longrightarrow 0.7Fe(OH)_2 \\ &0.54TiO_2 \Longrightarrow 0.54TiO_2 \\ &1.08Al^{3+} + 3.24OH^- \Longrightarrow 1.08Al(OH)_3 \\ &2.92H_4SiO_4 \Longrightarrow 2.92H_4SiO_4 \\ &0.56F^- \Longrightarrow 0.56F^- \end{aligned} \quad (37)$$

and 4.64 mol $OH^-$ are consumed by backtitration to neutral pH. This leaves 3.96 mol $H^+$ per mol of dissolved biotite not accounted for by backtitration. This part of $H^+$ should be added to the backtitration data.

Similarly, in the forward titration to the basic direction, 2.96 mol of $OH^-$ is consumed by dissolution reaction of 1 mol of biotite,

$$(KMg_{1.76}Fe_{0.7}Ti_{0.54})(Al_{1.08}Si_{2.92}O_{10})(OH_{0.44}F_{0.56}O) + 2.96OH^- + 11.92H_2O \Leftrightarrow K^+ + 1.76Mg^{2+} + 0.7Fe(OH)_2 + 0.54TiO_2 + 1.08Al(OH)_4^- + 2.92SiO_3^{2-} + 0.56F^- \quad (38)$$

Then in the backtitration to neutral conditions,

$$\begin{aligned} &K^+ \Longrightarrow K^+ \\ &1.76Mg^{2+} \Longrightarrow 1.76Mg^{2+} \\ &0.7Fe(OH)_2 \Longrightarrow 0.7Fe(OH)_2 \\ &0.54TiO_2 \Longrightarrow 0.54TiO_2 \\ &1.08Al(OH)_4^- + 1.08H^+ \Longrightarrow 1.08Al(OH)_3 \\ &2.92SiO_3^{2-} + 5.84H^+ + 2.92H_2O \Longrightarrow 2.92H_4SiO_4 \\ &0.56F^- \Longrightarrow 0.56F^- \end{aligned} \quad (39)$$

6.92 mol $H^+$ are consumed in the backtitration processes and this leaves 3.96 mol $H^+$ more are consumed in the backtitration per mol of dissolved biotite.

The results of forward and back titrations are summarized in Table 4. The amount of mineral dissolved was calculated according to the concentration of Si dissolved into the background solution. After the calibration of backtitration data, the titration curve is in the form of Figure 16b and it shows that most of the mineral dissolution has been calibrated.

However, the more $H^+$ consumption of Figure 16b at pH < 5 shows that the whole $H^+/OH^-$ consumption in the extreme pH areas can not be compensated by just backtitration. Other factors, cation exchange and proton exchange, will affect the consumption of $H^+$ in strongly acidic conditions as well. The theory can be explained by the following. In the forward titration, $M(OH)_3$, which represents the composition of mineral, will dissolve and consume $H^+$,

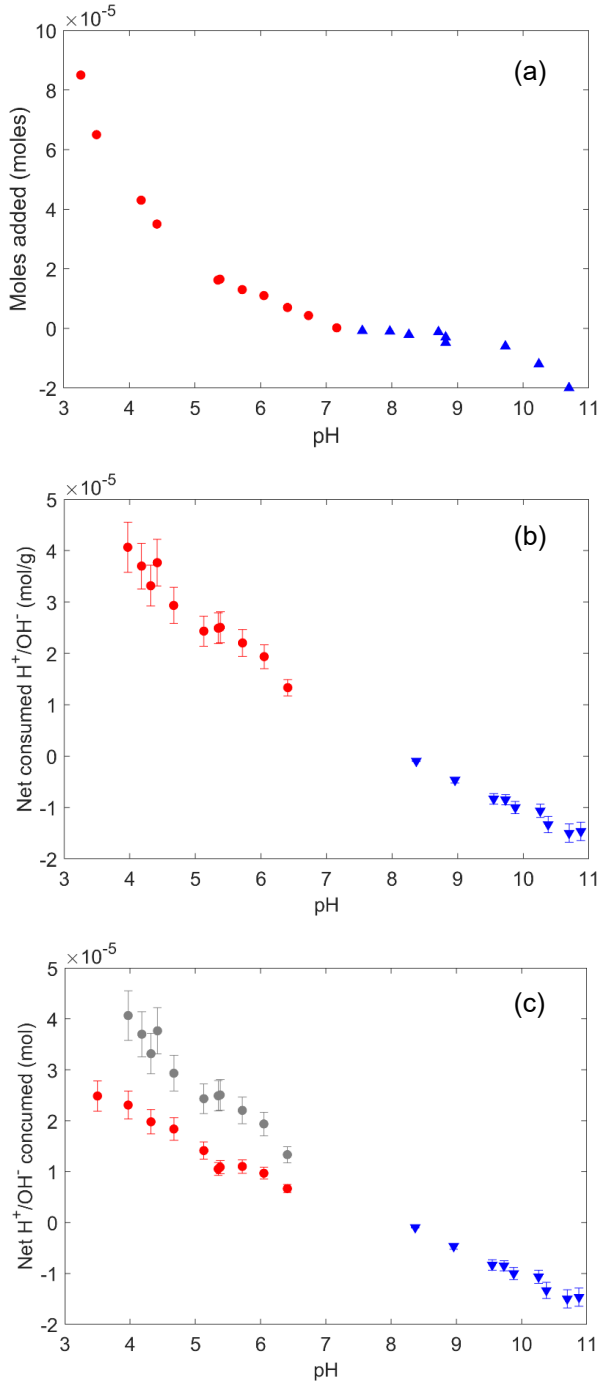


*Figure 16. (a) The moles of $HNO_3$ or NaOH consumed in the original titration results without calibration processes; (b) the amount of $HNO_3$ or NaOH consumed after calibration with backtitration results; (c) the net consumed amount of $HNO_3$ or NaOH calibrated with backtitration, cation exchange and proton exchange results.*

$$M(OH)_3 + 3H^+ \Leftrightarrow M^{3+} + 3H_2O \quad (40)$$

In the backtitration to the neutral conditions, $OH^-$ will be consumed,

$$M^{3+} + 3OH^- \Leftrightarrow M(OH)_3 \quad (41)$$

In the ideal condition, the amount of $OH^-$ consumed in the backtitration can indicate all the amount of $H^+$ consumed by mineral dissolution. However, because of the existence of cation exchange reactions between the dissolved $M^{3+}$ and the $K^+$ on the surface of biotite,

$$3K_{biotite} + M^{3+} \Leftrightarrow M_{biotite} + 3K^+ \quad (42)$$

part of the dissolved $M^{3+}$ will be removed from the solution and this part of $M^{3+}$ will not be compensated by backtitration.

The proton exchange reaction is defined as the exchange reactions between $H^+$ and the surface $K^+$ of biotite,

$$K_{biotite} + H^+ \Leftrightarrow H_{biotite} + K^+ \quad (43)$$

The amount of sorption sites of biotite occupied by different cations can be calculated according to the measured selective coefficients of cation/proton exchange reactions and the equilibrium cation concentrations. The results (Table 5) show that $Al^{3+}$ is the most abundant cation that can react with the $K^+$ on biotite surface and the reactions of other cations can be omitted compared with $Al^{3+}$. Thus, the amounts of $Al^{3+}$ and $H^+$ were used for the calibrations of cation exchange and proton exchange reaction, respectively, to calculate the net consumed $H^+$ in the strong acidic region. The results are also summarized in Table 4.

After taking into account the calibrations of backtitration, cation exchange and proton exchange reactions, the net consumed amount of $H^+/OH^-$ is listed in the last column of Table 4 and the final titration curve is shown in Figure 16c.

*Table 4. Summary of the forward titration (mol), backtitration (mol), minerals dissolution (mol), cation exchange (mol), proton exchange (mol) data for calculating the net consumed $H^+/OH^-$ (mol)in the titration experiments. The quantities of the net consumed $H^+$ or $OH^-$ are calibrated by backtitration, mineral dissolution, cation exchange and proton exchange.*

| pH | Acid/Base added | Backtitration added | Mineral dissolution | Cation exchange | Proton exchange | Net consumed |
|---|---|---|---|---|---|---|
| Acid | | | | | | |
| 6.41 | 7.0E-06 | 3.3E-07 | -- | -- | -- | 6.7E-06 |
| 6.05 | 1.1E-05 | 1.3E-06 | -- | -- | -- | 9.7E-06 |
| 5.72 | 1.3E-05 | 2.0E-06 | -- | -- | -- | 1.1E-05 |
| 5.38 | 1.7E-05 | 4.0E-06 | 1.7E-06 | -- | -- | 1.1E-05 |
| 5.35 | 1.6E-05 | 3.8E-06 | 1.9E-06 | -- | -- | 1.1E-05 |
| 5.13 | 3.2E-05 | 7.7E-06 | 7.8E-06 | 2.4E-06 | 1.8E-09 | 1.4E-05 |

| | | | | | | |
|---|---|---|---|---|---|---|
| 4.67 | 4.3E-05 | 1.4E-05 | 8.4E-06 | 2.5E-06 | 4.3E-09 | 1.8E-05 |
| 4.32 | 6.0E-05 | 2.7E-05 | 1.1E-05 | 2.7E-06 | 8.1E-09 | 2.0E-05 |
| 3.97 | 8.5E-05 | 4.4E-05 | 1.5E-05 | 2.8E-06 | 1.5E-08 | 2.3E-05 |
| 3.50 | 9.3E-05 | 4.6E-05 | 1.9E-05 | 2.9E-06 | 1.9E-08 | 2.5E-05 |
| Base | | | | | | |
| 8.37 | 2.2E-06 | 1.7E-06 | -- | -- | -- | 4.8E-07 |
| 8.96 | 4.0E-06 | 1.7E-06 | 7.3E-07 | -- | -- | 3.1E-06 |
| 9.55 | 7.0E-06 | 2.8E-06 | 4.8E-07 | -- | -- | 4.7E-06 |
| 9.73 | 8.0E-06 | 3.8E-06 | 5.2E-07 | -- | -- | 4.8E-06 |
| 9.88 | 1.0E-05 | 5.0E-06 | 9.6E-07 | -- | -- | 6.0E-06 |
| 10.26 | 1.5E-05 | 9.7E-06 | 1.9E-06 | -- | -- | 7.3E-06 |
| 10.38 | 2.0E-05 | 1.3E-05 | 2.6E-06 | -- | -- | 9.3E-06 |
| 10.70 | 3.0E-05 | 2.3E-05 | 5.1E-06 | -- | -- | 1.3E-05 |
| 10.88 | 4.0E-05 | 3.3E-05 | 6.8E-06 | -- | -- | 1.4E-05 |

*Table 5. The amount of sorption sites occupied by cations on converted biotite.*

| pH | Cation occupancies (meq/Kg) | | | | | |
|---|---|---|---|---|---|---|
| | H | K | Ca | Mg | Na | Al |
| 5.13 | 0.0037 | 4.9 | 0.029 | 0.120 | 0.028 | 14.4 |
| 4.67 | 0.0087 | 4.1 | 0.020 | 0.096 | 0.190 | 15.1 |
| 4.32 | 0.016 | 3.4 | 0.012 | 0.076 | 0.013 | 16.0 |
| 3.97 | 0.030 | 2.8 | 0.009 | 0.060 | 0.075 | 16.5 |

### 4.1.4 Sorption edge and sorption isotherm results

The sorption edge measurements were carried out by measuring the sorption of $10^{-9}$ M total Se(IV) with a radioactive Se-75 tracer on converted biotite in 0.01 M $KClO_4$ solution. Figure 17 (a) shows the experimental results and clear strong pH dependence of Se(IV) sorption was observed. This indicates that the sorption of Se(IV) ions on biotite surface undergoes the surface complexation mechanism.

The sorption isotherm experimental results (Figure 17, b) show a clear increasing trend of $K_d$ values with the decrease of Se(IV) concentration from $10^{-3}$ to $10^{-10}$ M. Two platforms exist at the low concentration area ($10^{-10}$ ~$10^{-8}$ M) and high concentration area ($10^{-6}$ ~ $10^{-3}$ M). This may indicate the change of sorption mechanisms when concentration changed.

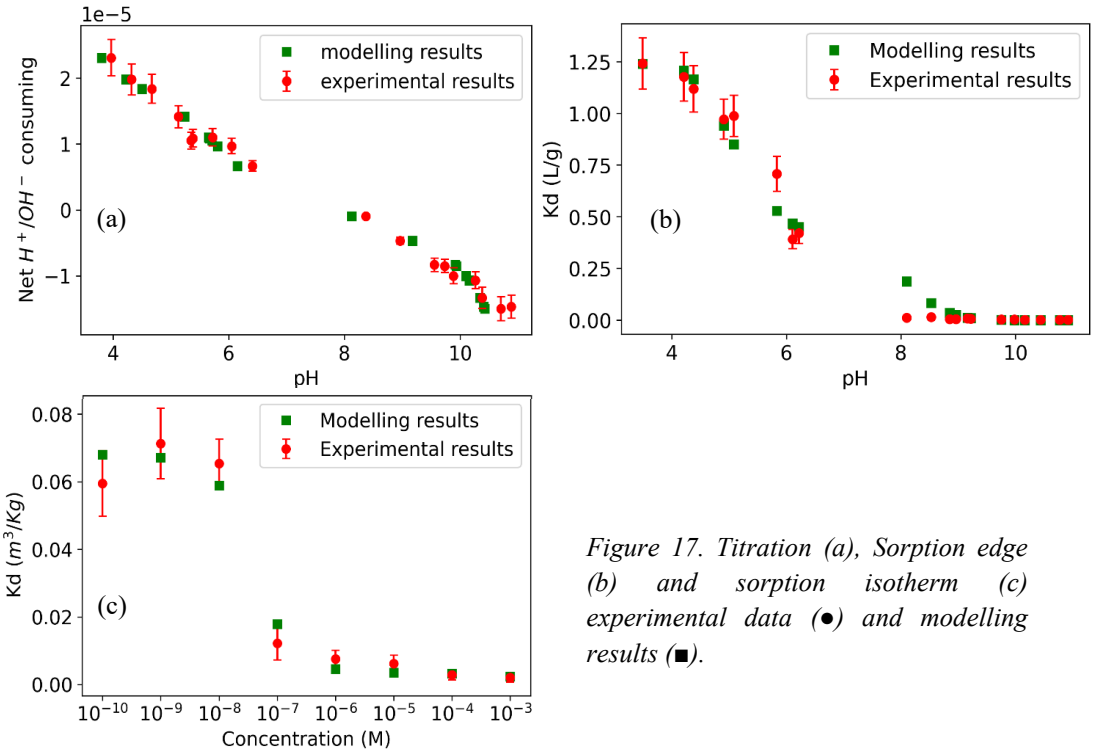


*Figure 17. Titration (a), Sorption edge (b) and sorption isotherm (c) experimental data (●) and modelling results (■).*

### 4.1.5 Analysis with multi-site surface complexation model and validation

The titration results were modelled in terms of protonation/deprotonation reactions (Equations (2) and (3)). The reaction constants can be described without an electrostatic term like,

$$K_{protonation} = \frac{[\equiv SOH_2^+]}{[\equiv SOH] \cdot \{H^+\}} \tag{44}$$

and

$$K_{deprotonatin} = \frac{[\equiv SO^-] \cdot \{H^+\}}{[\equiv SOH]} \tag{45}$$

where [] represents concentrations in M and {} represents activities. Table 6 (right) shows the protonation and deprotonation reactions of the assumed three kinds of sorption sites with the respective modelled reaction constants. The basic parameters of modelling such as site types, site densities and SSA were listed in Table 6 (left) and these basic parameters were fixed in the whole modelling procedures.

The sorption edge results were modelled with the surface complexation reactions between the strong sorption sites ≡$S^S$OH and the three different Se(IV) species as shown in Figure 15 right in the experimental pH range from 3 to 11. Depending on the distributions of the strong sorption sites in the same pH range as shown in Figure 18 left, different surface complexation reactions were assumed in different pH ranges.

*Table 6. Basic parameters used in the modelling of titration and sorption data (left); and the protolysis reactions of hydroxyl surface functional groups (≡SOH) and the corresponding reaction constants (right).*

| Parameter | Biotite |
|---|---|
| SSA(m2/g) | 1.0323 |
| Mass (g) | 0.5 |
| Sorption sites densities (sites/nm$^2$) | 0.00068 (S_sOH) |
| | 3.2 ($S^{w1}OH$) |
| | 1.4 ($S^{w2}OH$) |
| CEC (meq/Kg) | 12.64 |

| Protolysis reactions | log K |
|---|---|
| $\equiv S^SOH + H^+ \Leftrightarrow \equiv S^SOH_2^+$ | 5.05 |
| $\equiv S^SOH \Leftrightarrow \equiv S^SO^- + H^+$ | -8.78 |
| $\equiv S^{W1}OH + H^+ \Leftrightarrow S^{W1}OH_2^+$ | 5.05 |
| $\equiv S^{W1}OH \Leftrightarrow \equiv S^{W1}O + H^+$ | -8.78 |
| $\equiv S^{W2}OH + H^+ \Leftrightarrow \equiv S^{W2}OH_2^+$ | 6.10 |
| $\equiv S^{W2}OH \Leftrightarrow \equiv S^{W2}O^- + H^+$ | -11.22 |

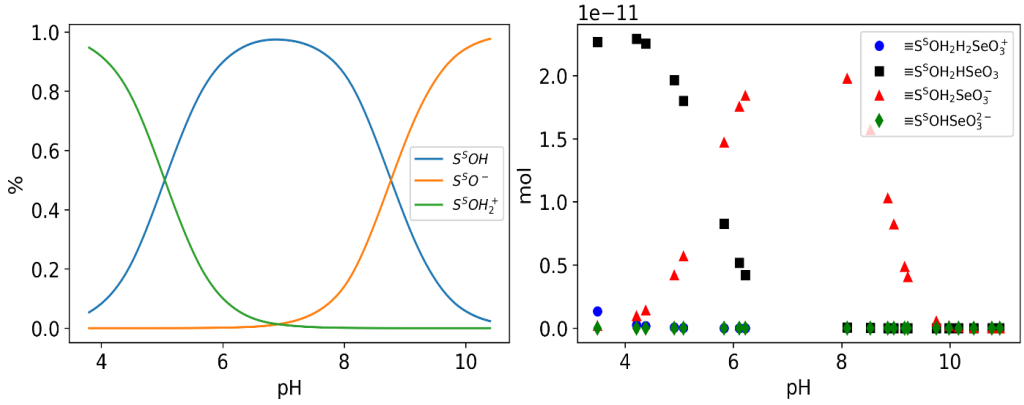


*Figure 18. The strong sorption sites distribution as a function of pH (left) and the distribution of different sorption species on the surface of biotite as a function of pH (right).*

At pH > 9, $SeO_3^{2-}$ is the main Se species and reaction,

$$SeO_3^{2-} + \equiv S^SOH \Leftrightarrow \equiv S^SOHSeO_3^{2-} \quad (46)$$

is considered as the main reaction as $SeO_3^{2-}$ and $\equiv SOH/\equiv SO^-$ are the main species at this pH conditions. When pH is between 7 and 9, both $SeO_3^{2-}$ and $HSeO3^-$ exist in the aqueous phase. The reaction between $HSeO3^-$ and $\equiv S^SOH$,

$$HSeO3^- + \equiv S^SOH \Leftrightarrow S^SOH_2SeO_3^- \quad (47)$$

will become more and more important with pH decreasing.

At pH between 4 and 7, the amount of $SeO_3^{2-}$ is minimal and the protonated sorption hydroxyl groups $\equiv S^SOH_2^+$ will become popular. The complexation reaction is expressed as,

$$HSeO_3^+ + H^+ + \equiv SOH \Leftrightarrow \equiv S^SOH_2HSeO_3 \quad (48)$$

When pH < 4, the $H_2SeO_3$ species will appear and the complexation between $H_2SeO_3$ and $\equiv S^SOH_2^+$ will be considered,

$$H_2SeO_3 + H^+ + \equiv S^SOH \Leftrightarrow \equiv S^SOH_2H_2SeO_3^+ \quad (49)$$

The selectivity coefficients of the complexation reactions (Equation (46) to (49)) calculated from the modelling processes are summarized in Table 7, and the modelling data are shown in Figure 17 (b). One can summarize from the trend of the selective coefficients of the complexation reactions that the complexation ability of different Se species follows in the order $H_2SeO_3$ > $HSeO3^-$ > $SeO_3^{2-}$. This result is in accordance with the calculated sorption energies by molecular modelling.

The sorption isotherm results were modelled based on the parameters from titration and sorption edge modelling results as well as the surface complexation reactions between $HSeO3^-$ and $\equiv S^{W1}OH$ / $\equiv S^{W2}OH$ sorption sites, as shown in Table 7. In the high concentration region, where most of the surface complexation reactions happen on the two types of weak sorption sites, $HSeO3^-$ is regarded as the main Se species. One reason is that at the experimental pH conditions (7.7), $HSeO3^-$ is the most abundant Se species; the other reason is that $HSeO3^-$ has more complexation ability than $SeO_3^{2-}$, as we got from the modelling of sorption edge results.

*Table 7. Surface complexation reactions between different Se species with strong and weak sorption sites. The selectivity coefficients are calculated by the multi-site surface complexation model.*

| Reactions | log K |
|---|---|
| $SeO_3^{2-} + \equiv S^SOH \Leftrightarrow \equiv S^SOHSeO_3^{2-}$ | -2.23 |
| $HSeO_3^- + \equiv S^SOH \Leftrightarrow \equiv S^SOH_2SeO_3^-$ | 7.89 |
| $H^+ + HSeO_3^- + \equiv S^SOH \Leftrightarrow \equiv S^SOH_2HSeO_3$ | 13.46 |
| $H^+ + H_2SeO_3 + \equiv S^SOH \Leftrightarrow \equiv S^SOH_2H_2SeO_3^+$ | 13.02 |
| $HSeO_3^- + \equiv S^{W1}OH \Leftrightarrow \equiv S^{W1}OH_2SeO_3^-$ | 2.78 |
| $H^+ + HSeO_3^- + \equiv S^{W1}OH \Leftrightarrow \equiv S^{W1}OH_2HSeO_3$ | 3.78 |
| $HSeO_3^- + \equiv S^{W2}OH \Leftrightarrow \equiv S^{W2}OH_2SeO_3^-$ | 2.48 |
| $H^+ + HSeO_3^- + \equiv S^{W2}OH \Leftrightarrow \equiv S^{W2}OH_2HSeO_3$ | 2.62 |

The modelling results are shown in Figure 17 (c). The site occupation calculations show that the site density of the strong sorption sites is 0.00068 sites/nm$^2$, which is much lower than that of the two types of weak sorption sites. This is in accordance with the assumption that the strong sorption sites dominate the sorption behaviours in the low concentration region while the weak sorption sites dominate the sorption behaviours in the high concentration region.

The multi-site surface complexation model developed in this work was validated by the sorption isotherm data measured at pH 9.5. The best fit was achieved at pH 9.34 which is in fair

agreement with the experimental conditions. This proves that the surface complexation model developed here could be used to describe the Se(IV) sorption on bedrock over a pH range from 7.5 to 9.5 which covers most of the pH values of groundwaters in bedrocks of a nuclear waste repository.

### 4.1.6 Molecular modelling of surface sites and reactions

The structures of the basal and edge surfaces of phlogopite were investigated by DFT molecular modelling. The basal (001) and edge (110) surfaces were identified as the active sorption surface of Se species. The structures of the sorption sites on corresponding surfaces are shown in Figure 19. These two kinds of sorption sites were studied as weak sorption sites in the multi-site surface complexation modelling. By optimizing the sorption geometries, the number of sorption site for sorption of Se species were calculated. The sorption site density of the basal (001) surface was estimated to be 3.2 sites/nm$^2$ and the sorption site density of the edge (110) surface was estimated as 1.4 sites/nm$^2$ (Table 6).

A molecular level illustration of the sorption of the three Se species, $SeO_3^{2-}$, $HSeO_3^-$ and $H_2SeO_3$ on the two kinds of sorption sites were studied and the optimized bonding geometries are shown in Figure 19. According to the modelling process, electron transfer reactions happen between the biotite surface and Se(IV) species when coordination reactions happen on the (110) edge surface, and during the reaction processes, anionic and neutral Se(IV) species can transfer to cationic species $HSeO_2^+$. In contrast, at the (001) basal surface, electron transfer processes are not thought to be dominant.

The energies of the corresponding surface sorption reactions are summarized in Table 8. The results indicate that Se will be sorbed on phlogopite surface via the oxygen atom of the oxyanion. The sequence of the sorption energies for both types of sorption sites follow the order of $H_2SeO_3$ < $HSeO_3^-$ < $SeO_3^{2-}$, which is in the same order of the logK values of the reactions calculated by the multi-site surface complexation model. The result indicates that HeSeO3 is the most favourable sorption Se species onto phlogopite surface and then $HSeO_3^-$, while $SeO_3^{2-}$ is the least favourable. Because of the rare occurrence of $H_2SeO_3$ in normal groundwaters, this explains the common experimental observations that Se will be sorbed in the form of $HSeO_3^-$ by many researchers.

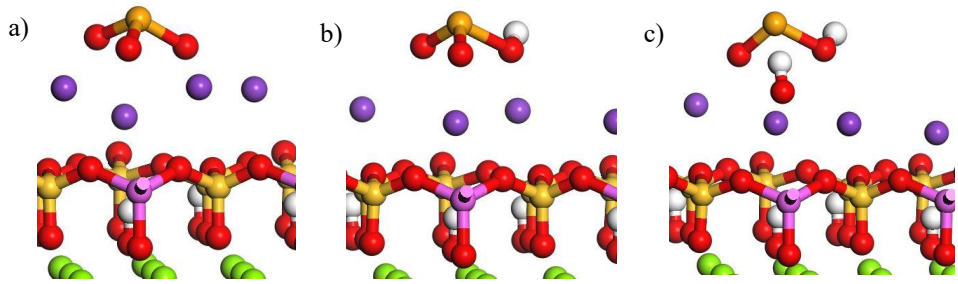

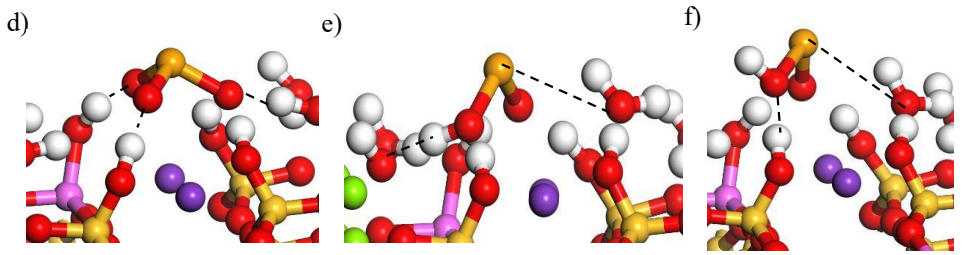


*Figure 19. Optimized sorption geometries of Se species: $SeO_3^{2-}$, $HSeO_3^-$ and $H_2SeO_3$ on phlogopite basal (a, b, c) and edge (d, e, f) surfaces.*

*Table 8. Sorption energies (eV) calculated in the DFT molecular modelling of Se (IV) species on phlogopite basal (001) and edge (110) surfaces.*

| Se species | Phlogopite | | |
|---|---|---|---|
| | **(110)** | **(110)** | **(001)** |
| | –O–Se | –Se–O | –O–Se |
| $Se(IV)O_3^{2-}$ | 4.6 | 6.4 | 5.7 |
| $HSe(IV)O_3^-$ | -1.8 | 4.5 | 3.4 |
| $H_2Se(IV)O_3$ | -5.2 | 0.7 | -2.3 |

## 4.2 Results of diffusion studies

### 4.2.1 Characterization results of the intact rock sample

The intact granitic rock sample used in the electromigration experiment was collected from Äspö underground laboratory (borehole KLX11F, 17m) in collaboration with Linnaeus University. The geometry of the rock sample was determined with a calliper (1.12cm length, 5 cm diameter). The lithology distribution of the rock sample was quartz monzodiorite (95.5%) and fine-grained granite (4.5%). More detailed information could be checked in the report Mattsson et al. (2007).

The porosity of the intact rock sample was determined by the water weight difference method. The weight of the background electrolyte saturated rock sample in the open air was followed as a function of time until the surface of the rock sample was fully dried. The drying curve is shown in Figure 20. The orange lines represent the process of out-surface dryness while the green line represents the evaporation of the pore water. The intersection of the two lines indicates the weight of the rock sample with totally dry surface when pore water has been fully evaporated. The porosity of the rock sample was calculated by the difference of the weight of rock sample with dried surface (evaluated from Figure 20) and the weight of totally dried rock sample as well as the density of the electrolyte. The porosity determined was 0.7%.

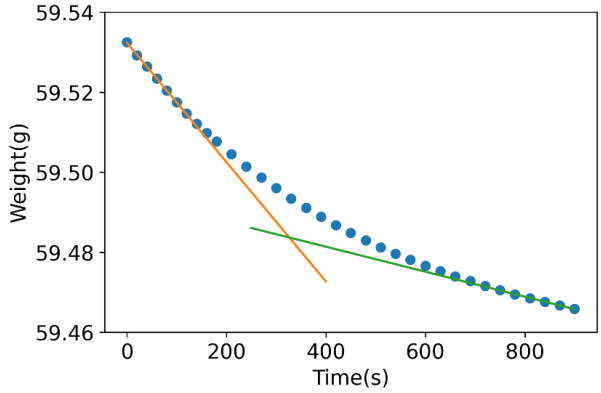


*Figure 20. The weight of the water saturated rock sample measured in the open air as a function of drying time.*

### 4.2.2 Updated electromigration device presentation

The updated electromigration device, designed based on the ideas listed in Section 3.3.1, is shown in Figure 21 left. The volume of the source and recipient chambers, built with poly (methyl methacrylate) (PMMA), is 152 mL and the volume of the two electrode chambers at both ends is 250 mL. Compared with the pore volume of the rock sample, the volume of the chambers can be considered as infinitely large. Thus, the concentration change of the tracer in the source chamber can be regarded as constant during the whole experimental period.

The electrodes in the four chambers, connected and controlled by a potentiostat in a four-electrode system, were made of titanium metal. A sample holder (Figure 21 right), made of PMMA, was also designed to make sure that all tracer ions migrate only through the intact rock sample by its micropores. A similar holder design was also applied to the two filters which have similar mineralogical compositions of the rock sample. The two filters were used to separate the two electrode chambers from the source/recipient chambers.

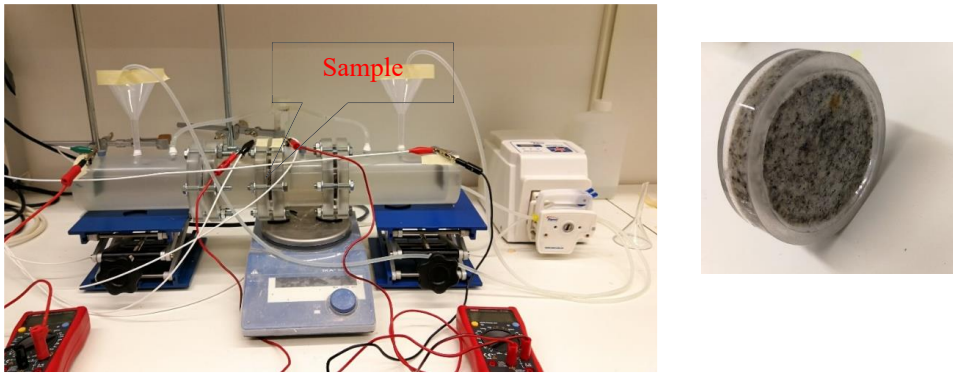


*Figure 21. Setup of the electromigration experiments (left). The sample is in the middle of the setup between the source chamber and the recipient chamber. At both ends are the two electrode chambers separated by two rock filters from the tracer chambers. Right is the Sample/filter holder designed for the electromigration setup.*

Due to the introduction of the potentiostat (Figure 14) and the stabilization of the pH values of the background electrolyte by adding $NaHCO_3$ buffer, the modified device has the functions of voltage-self-controlling, continuous-current-recording and solution-pH-stabilization which are lacking in former designs. It enables to provide more accurate and reproducible results of electromigration experiments. Long term running of the device also becomes possible, because the voltage over the rock sample will be adjusted automatically by the device itself to keep a constant value whenever the resistance of the rock sample changes.

### 4.2.3 New models for accurate electromigration analysis

The ideal plug-flow model used by former researchers for analysing electromigration experimental results contains lots of assumptions, which gives large uncertainties in parameter identifications. To interpret the experimental results more accurately, we developed an advection-dispersion model that accounts for not only the dominant effect of electromigration but also the contribution of electroosmosis and dispersion on ionic transport. The processes of the modelling development are shown briefly below.

The mass balance on the ions over a thin shell of the rock sample perpendicular to the direction of mass transport follows the general convection-dispersion equation which is expressed as,

$$(\varepsilon_{TS} + \rho_d K_d)\frac{\partial c}{\partial t} = -\varepsilon_T v_c \frac{1}{\tau^2}\frac{\partial c}{\partial x} + \varepsilon_T \delta_D D \frac{1}{\tau^2}\frac{\partial^2 c}{\partial x^2} \tag{50}$$

where $v_c$ is the convection velocity composed of both $v_{em}$ and $v_{eo}$, i.e. $v_c = v_{em} + v_{eo}$, $\rho_d$ is the dry bulk density of the rock sample, $K_d$ is the distribution coefficient, $\varepsilon_{TS}$ is the porosity available for both transport and storage, $\varepsilon_T$ is the porosity associated with the transport, $\delta_D$ is the constrictivity, considered to depend on the ratio of the diameter of the ions to the pore diameter, and $\tau$ is the tortuosity, defined as the ratio between the real distance of the transport path and the experimentally measured end to end distance.

With the assumption of a linear sorption isotherm, a retardation factor is defined as,

$$R = 1 + \frac{\rho_d K_d}{\varepsilon_{TS}} \tag{51}$$

Then we introduce an effective convection velocity

$$v_c^e = \frac{\varepsilon_T}{\tau^2} v_c \tag{52}$$

and an effective dispersion coefficient

$$D^e = F_f D \tag{53}$$

with the formation factor defined as

$$F_f = \frac{\varepsilon_T \delta_D}{\tau^2} \tag{54}$$

Then the Equation (50) reduces to

$$\varepsilon_{TS} R \frac{\partial c}{\partial t} = -v_c^e \frac{\partial c}{\partial x} + D^e \frac{\partial^2 c}{\partial x^2} \tag{55}$$

To facilitate analysis of experimental results, it is often preferable to define an apparent convection velocity

$$v_c^a = \frac{v_c^e}{\varepsilon_{TS} R} \tag{56}$$

and an apparent dispersion coefficient

$$D^a = \frac{D^e}{\varepsilon_{TS} R} \tag{57}$$

Consequently, Equation (55) reduces to

$$\frac{\partial c}{\partial t} = -v_c^a \frac{\partial c}{\partial x} + D^a \frac{\partial^2 c}{\partial x^2} \tag{58}$$

Equation (55) can be solved with the initial condition,

$$c(x, 0) = 0 \tag{59}$$

and the boundary conditions,

$$c(0, t) = c_L(t) \tag{60}$$

and

$$c(L, t) = c_R(t) \tag{61}$$

where $L$ is the length of the rock sample; $c_L$ and $c_R$ are the tracer concentration in the source and recipient chambers, respectively.

The evolution of $c_L$ with time can be determined in terms of a macroscopic mass balance over the source chamber as,

$$V_L \frac{dc_L}{dt} = -AN^e|_{x=0} \tag{62}$$

along with the initial condition:

$$c_L(0) = c_0 \tag{63}$$

where $V_L$ is the volume of the left chamber and $A$ is the cross-section area of the rock sample.

Similarly, the evolution of $c_R$ with time can be described by a macroscopic mass balance over the right chamber, which receives the tracer, i.e.,

$$V_R \frac{dc_R}{dt} = AN^e|_{x=l} \tag{64}$$

along with the initial condition,

$$c_R(0) = 0 \tag{65}$$

Equations (58) to (65) give a full description of the dynamic process of electromigration, which can be solved by the Laplace transform method. The detailed solution process is illustrated in Paper (IV). The Laplace transformed solution of $c_R$ is

$$\overline{c_R} = -\frac{\exp\left(\frac{Pe}{2}\right)\frac{Scsch(S)}{Pe}}{\left[\frac{1}{2} + \beta_L s + \frac{Scoth(S)}{Pe}\right]\left[\frac{1}{2} - \beta_R s - \frac{Scoth(S)}{Pe}\right] + \left[\frac{Scsch(S)}{Pe}\right]^2}\beta_L c_0 \tag{66}$$

where $s$ is the Laplace variable, $S$ is a $s$-dependent variable defined as,

$$S = \frac{Pe}{2}\sqrt{1 + \frac{4\tau_A s}{Pe}} \tag{67}$$

$Pe$ is the Péclet number, $\beta_L$ and $\beta_R$ are the relaxation times of the source and recipient chambers, respectively.

The inverse Laplace transform of Equation (66) gives the tracer concentration $c_R$ at the recipient chamber and it can, for a given experimental setup, be generally written as,

$$c_R = f(v_c^e, D_e, \varepsilon_{TS}R, c_0, t) \tag{68}$$

This result indicates that the numerical solution of $c_R$, obtained by use of e.g. De Hoog algorithm (de Hoog et al., 1982) to numerically transform Equation (66) back to the time domain, would depend only on $v_c^e, D_e$ and $\varepsilon_{TS}R$. As a consequence, these parameters can readily be evaluated by fitting the numerical solution $c_R$ to the measured data of the breakthrough curve using e.g. a nonlinear least squares algorithm supplemented with suitable lower and upper bounds.

### 4.2.4 Electromigration experimental results and model analysis

The experimental conditions and critical parameters of the electromigration device were summarised in Table 2. The quinoxaline tracer was tested for the determination of electroosmosis. The iodide, which was regarded as a non-sorbing ion on mineral surfaces, was tested secondly because iodide was the most tested ion in the former electromigration studies. Thirdly, Se(IV) species, which are slightly sorbing ions according to our sorption studies, were run with our electromigration device. The results running with different tracers were modelled with three models we developed in our work, the ideal plug-flow model, advection-dispersion model and reactive transport model.

#### 4.2.4.1 Electroosmosis measurement results

Quinoxaline was used as the tracer for measuring the effect of electroosmosis on ionic transport inside the intact rock sample. After 5 days of continuous running for several times before the running with Se and I tracer, no obvious detection of quinoxaline was observed in the recipient chamber. The highest observation was that electroosmosis might account for 4.1% of the total electromigration processes compared with the running with iodide tracer afterwards. However,

this observation just appeared once. It was, therefore, deemed that the effect of electroosmosis can be omitted in the electromigration processes under our experimental conditions.

#### 4.2.4.2 NaI and $Na_2SeO_3$ experimental results and modelling with IPF model

Two voltages (2V and 4V) were applied and controlled automatically (±0.01V) by the potentiostat over the rock sample. Thus, the potential gradients of the rock sample were 179 V/m and 357 V/m, respectively. After following the concentration of the tracer ions in the recipient chamber for about 2 days, we got the breakthrough curves of these tracer ions as a function of experimental time recorded by the potentiostat. The experimental results of the tracer ions as well as the modelling results with different models are shown in Figure 22. The results show that iodide can migrate through the rock sample more quickly than selenite ions, which can be seen from the breakthrough time of these tracers clearly. Before the breakthrough time, the concentration of tracer ions in the recipient chamber remained apparently at the background level. This indicates that the electromigration device was in a good condition of tightness and thus all the tracer ions have migrated through the rock sample by the connective pore network.

In order to interpret the experimental results more precisely and quantitatively, different modelling methods were applied to fit the experiment results and derive diffusion parameters. The ideal plug-flow model was tried first, since it is the simplest and most commonly used modelling method to interpret electromigration results. One just needs to make a linear regression line of the late-time data of the breakthrough curve over which the tracer concentration increases seemly at a constant rate and a pseudo-steady-state was considered to be established (Figure 22). The intercept of the regression line with the time coordinate ($t_B$) gives the breakthrough time of the tracer ions, i.e. $t_B \approx \tau_A$, where $\tau_A$ is the characteristic advection time. The slope of the linear regression line ($\kappa$) gives approximately the concentration change rate of the tracer ions in the recipient chamber, i.e. $\kappa \approx c_0/\beta_R$. As a result of these assumptions, the effective diffusion coefficient of the tracer ions can be calculated with Equation (35). To better describe the diffusion properties of the intact rock sample, formation factor, $F_f$, which describes the pore system configuration and the rate of transport through the pore system of the rock sample, is also calculated by Equation (24) in this thesis. The calculated results for both tracer ions are summarised in Table 9.

*Table 9. Summary of the modelling results of molecular effective diffusion coefficients, $D_e$ and formation factors, $F_f$, applied with the ideal plug-flow model, advection-dispersion model and reactive transport model.*

| | Iodide | | Se(IV) species | |
|---|---|---|---|---|
| Model applied | $D_e(10^{-14}\,m^2s^{-1})$ | $F_f$ $(10^{-5})$ | $D_e(10^{-14}\,m^2s^{-1})$ | $F_f$ $(10^{-5})$ |
| Ideal plug-flow model | 8.33±3.25 | 4.06±1.59 | 2.30±0.89 | 2.30±0.89 |
| Advection-dispersion model | 11.5±0.60 | 5.61±0.29 | 3.50±0.86 | 3.50±0.86 |
| Reaction transport model | 12.4±1.05 | 6.06±0.51 | 3.75±0.35 | 3.75±0.35 |

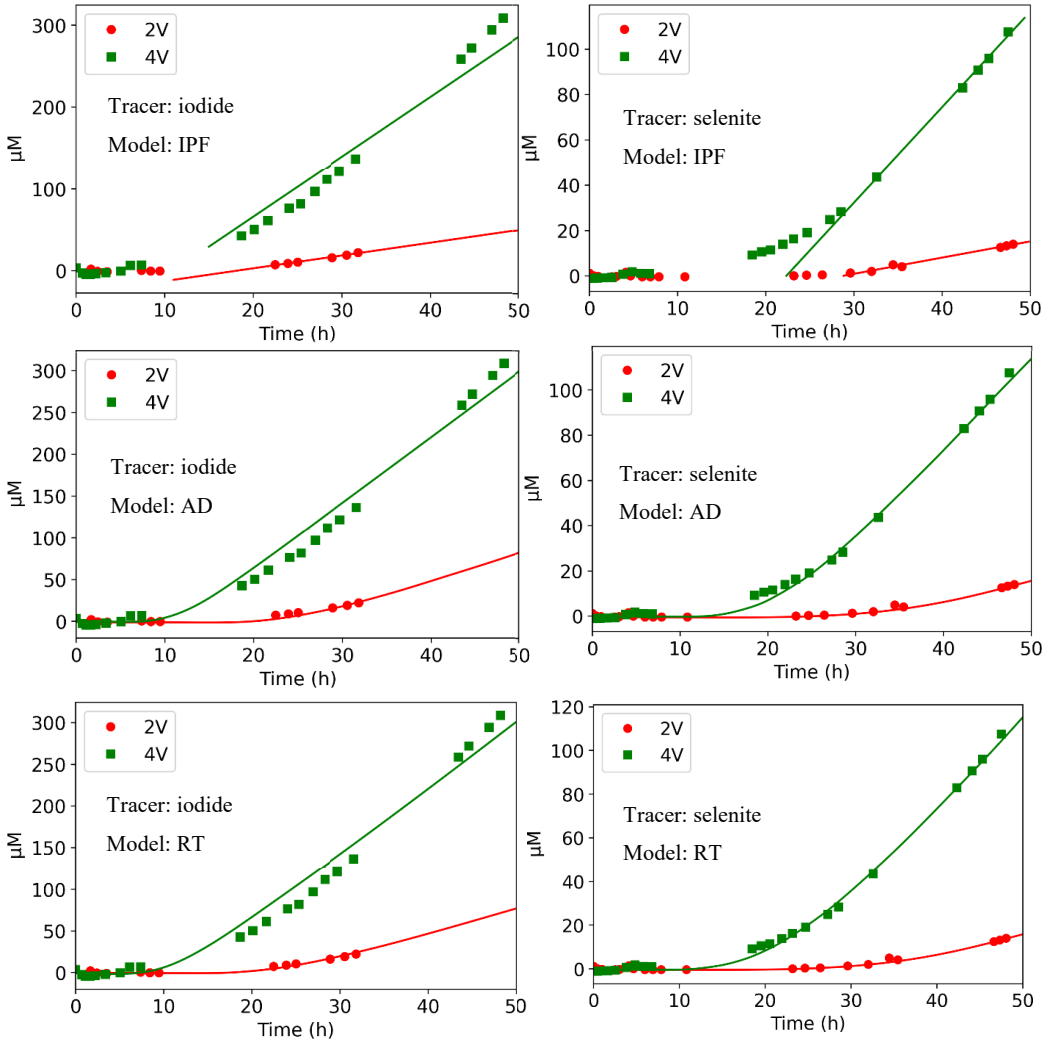


*Figure 22. The concentration of iodide (left) and Se(IV) species (right) (µM) followed in the recipient chamber as a function of experimental time and the modelling results with ideal plug-flow model (IPF), advection-dispersion model (AD) and reactive transport model (RT).*

#### 4.2.4.3 Modelling with advection-dispersion model

According to the above results, the ideal plug-flow model can only be used to give a quick but rough estimate of the parameters such as $v_e, D_e, F_f$ and $R$ etc. The results can be used in defining the lower and upper bounds of the corresponding parameters. To perform a more precise analysis, the advection-dispersion model developed in this work is recommended because it takes into account more influencing factors in the electromigration processes, i.e. electromigration, electroosmosis and dispersion. By numerically transform Equation (66) to the

time domain and fitting the solution $c_R$ to the experimental data of both iodide and selenite, one can get the modelling results as shown in Figure 22.

The difference of the modelling results between the ideal plug-flow model and the advection-dispersion model is quite clear. The ideal plug-flow model simply makes a linear regression line of the data at which a pseudo-steady-state seems to be achieved after breakthrough time. However, it is noted that the measured breakthrough curves show a clear curvature at the moment around the breakthrough time, which is certainly overestimated by the ideal plug-flow model. This indicates that dispersion played a non-negligible role in the ionic transport through the rock sample. As a consequence, the application of the ideal plug-flow model for parameter identification can be problematic because it ignores the effect of dispersion and uses only a small part of the late-time experimental results. The advection-dispersion model, on the contrary, analyses the whole breakthrough curve instead, and more factors that can affect the results can be taken into account when fitting the breakthrough curve with the advection-dispersion model.

#### 4.2.4.4 Modelling with the reactive transport model

The inherent ignorance in the advection-dispersion model of the speciation of the aqueous solution and ionic equilibrium (aqueous chemistry) gives rise to the question that the neglect of aqueous chemistry may influence the results of parameter identification to some extent. To examine how severe the deviations could be, a reactive transport model tailored for the electromigration cell (Figure 11) was developed. The method is to reformulate the advection-dispersion model by replacing $c$ as $c_i$, the concentration of the $i$th species, in the governing equations as well as in the initial and boundary conditions, in addition to include mass-action equations, mass and charge balance equations etc., as the geochemical model of PHREEQC does. The implementation of such a reactive transport model is not straightforward, especially in the cases considering individual diffusion coefficients for the solute species. To address this problem in a simple means, one can couple the Iphreeqc modules with the Python script, same as we performed in developing the multi-site surface complexation model. The coupling of Iphreeqc modules with Python script facilitates specific treatment of the boundary conditions and calculation of the reactive transport in a stepwise and coupled manner.

The flux due to the gradients in concentration, electric potential as well as electroosmosis and dispersion can be written with,

$$N_i^e = -D_i^e\left(\frac{\partial c_i}{\partial x} + \frac{z_i e c_i}{k_B T}\frac{D_{m,i}^e}{D_i^e}\frac{\partial \psi}{\partial x}\right) \tag{69}$$

where $N_i^e$ is the effective flux of ion i, $D^e$ is the effective dispersion coefficient, $c$ is the concentration, $x$ is the distance, $z$ is the charge number, $e$ is the electron charge, $k_B$ is the Boltzman constant, $T$ is the absolute temperature, $D_m^e$ is the effective molecular diffusion coefficient, $\psi$ is the electric potential.

At this moment, the development of the reactive transport model has not been fully completed yet. However, PHREEQC provides a module for electromigration which we can use for

calculations of chemical reactions in electromigration processes. In order to utilize the PHREEQC electromigration module, we assumed that the ratio of $D_{m,i}^{e}/D_{i}^{e}$ is a constant, based on the expectation that the electroneutrality condition is more dominant than the ratio of $D_{m,i}^{e}/D_{i}^{e}$ in determining the local mass flux. Thus, Equation (69) can be written as

$$N_i^e = -D_i^e\left(\frac{\partial c_i}{\partial x} + \frac{z_i e c_i}{k_B T}\frac{\partial \psi'}{\partial x}\right) \tag{70}$$

with

$$\psi' = \frac{D_{m,i}^{e}}{D_i^e}\psi \tag{71}$$

The introduction of the modified electric potential $\psi'$, instead of $\psi$, makes it possible to use the PHREEQC module of electromigration for interpretation of our experimental results. The modelling results are also summarized in Figure 22 and Table 9.

By comparing all the modelled results shown in Table 9, it is seen that the ideal plug-flow model show a larger difference than the other two models in both the mean values and uncertainties. This is caused by the neglect of the dispersion process and other simplifications behind the model. The advection-dispersion model gives nearly the same estimates of the parameters as the reactive transport model. The findings suggest that the effect of aqueous chemistry is unimportant compared with the effect of electromigration and dispersion in governing ionic transport in the electromigration processes. The advantage of the reactive transport model is its capability and flexibility in accounting for the effect of water chemistry, individual diffusion coefficients of the solute species and multiple sorption mechanisms simultaneously, giving a more detailed analysis of the ion transport processes. However, the reactive transport model is more time consuming in computation and more intricate in implementation. As a consequence, the advection-dispersion model is recommended, in our opinion, to be in the first place for interpreting the electromigration experimental results.

# 5 Conclusions and Outlook

The sorption and diffusion behaviour of Se(IV) species in granitic rock samples were investigated with both experimental and modelling methods. A multi-site surface complexation model was developed based on the titration data, sorption edge data and sorption isotherm data measured in laboratory to illustrate the sorption processes of Se(IV) species on Grimsel granodiorite rock samples and its main minerals, especially biotite. An electromigration device was updated and tested by running with iodide and Se(IV) ions to determine the diffusion and sorption properties of them in intact granitic rock samples. The electromigration experimental results were modelled with the traditional ideal plug-flow model and two newly developed models, the advection-dispersion model and reactive transport model.

The $K_d$ values of Se(IV) ions on Grimsel granodiorite and its main minerals were determined by batch sorption experiments. The sorption abilities of these rock and mineral samples followed the order: biotite > K-feldspar > Grimsel granodiorite ≈ plagioclase > quartz. It was therefore assumed that the Se(IV) sorption on biotite could represent its sorption on granitic rock samples. SSA was found to play an important role in Se(IV) sorption because a linear relation between SSA and $K_d$ values were found for all the rock and mineral samples.

In order to develop a multi-site surface complexation model, three sets of experimental data were measured: titration data, sorption edge data and sorption isotherm data. The titration experiments were carried out in a batch-wise manner to measure the mineral surface site capacities and intrinsic surface protonation and deprotonation constants for the amphoteric ≡ $SOH$ surface sites of biotite from 3 to 11. To compensate for the effect of mineral dissolution, the forward titration results were calibrated with backtitration, cation exchange and proton exchange processes. The results show that backtitration is the main calibration to the $H^+/OH^-$ consumptions. The calculations of the amount of sorption sites occupied by cations on the biotite surface show that dissolved $Al^{3+}$ is the most abundant cation that is sorbed on the biotite surfaces. As a result, $Al^{3+}$ and $H^+$ occupancies were used as further cation exchange and proton change calibrations.

Sorption edge measurements were carried out by measuring the sorption of $10^{-9}$ M total Se with a radioactive Se-75 tracer on biotite from pH 3 to 11. Se(IV) sorption showed a strong dependency on the pH conditions of background solutions. The $K_d$ values of Se sorption on biotite were found to decrease when pH increases from 3 to 11.

Sorption isotherm measurements were carried out at around pH 7.7 from Se(IV) concentrations from $10^{-10}$ M to $10^{-3}$ M. The $K_d$ values were found to be increasing with the decreasing Se(IV) ion concentrations, however, two platforms were observed in the low and high concentration regions. A drastic change of $K_d$ happened at concentrations around $10^{-7}$ M.

A multi-site surface complexation model was derived by fitting a set of modelling parameters for all the experimental data. A kind of strong sorption sites and two kinds of weak sorption sites were assumed in the surface complexation modelling according to the DFT molecular modelling calculation results. A computer code PHREEQC coupled with Python was used for all the fitting and optimization processes. The fitting procedure was performed in an iterative

way until a group of parameters that is able to describe all the experimental results satisfyingly was found. The model was validated by the Se(IV) sorption data at pH ~9.5 and it describes well the $K_d$ values at both high and low concentration regions. This proves that the modelling methods shown in our work can be used to successfully derive a surface complexation model for the sorption of the radionuclides on the crystalline rock in deep geological repositories. In the future, the model could be used to validate the Se(IV) sorption in a wide range of groundwater conditions.

DFT molecular modelling was performed to provide surface site information for surface complexation modelling and to examine the complexation reactions happened on biotite surface. DFT molecular modelling was carried out by a CASTEP code implemented into Materials Studio Software. The modelling results showed two types of weak sorption sites on the biotite surfaces with site densities of 3.2 sites/nm$^2$ and 1.4 sites/nm$^2$. Thus, the structures of the sorption sites assumed in the surface complexation model were illustrated at the atomic level. The surface complexation reactions of different Se species at the two kinds of weak sorption sites were examined and corresponding sorption energies were calculated. The possible sorption reactions on the specific crystalline surfaces were estimated according to the sorption energies and the possible surface charge transfer reactions were also considered. The results deepened our understanding of the assumed reactions in the surface complexation model and provide theoretical support for the development of the surface complexation model.

The diffusion studies were performed with the electromigration method since it has been proved to be a simple and fast technique and can avoid problems encountered using crushed rock samples. A new electromigration device was developed by introducing a potentiostat to the traditional electromigration system and better control of the background solution pH conditions. By applying a four-electrode system, the potentiostat can keep the voltage over the rock sample to be constant during the experimental period by adjusting the overall voltage applied to the whole device automatically. The potentiostat can also record the current data which facilitates the analysis of the ion distribution and diffusion of different ions inside the rock sample.

The updated electromigration device was tested by running with three tracers: quinioxaline, iodide and Se(IV), under two different potentials, 2V and 4V, over the rock sample. The quinoxaline results indicate that the effect of electroosmosis can be omitted when analysing the electromigration results. In order to facilitate a more accurate interpretation of the experimental results than the traditional ideal plug-flow model which account only for the effect of electromigration, an advection-dispersion model was developed. The new model accounts for three dominant effects of ionic transport under the influence of a potential gradient, electromigration, electroosmosis and dispersion. Thus, the advection-dispersion model provides better parameter identification with smaller uncertainties than the ideal plug-flow model. To further develop the electromigration modelling method, a reactive transport model was developed by taking into account the effect of aqueous chemistry which was neglected in the advection-dispersion model. The $D_e$ values from ideal plug-flow modelling have larger uncertainties and they differ significantly from the new models. The advection-dispersion model can give nearly the same modelling results as the reactive transport model, however, the reactive transport model is more time-consuming in computation and more intricate in

implementation. Thus, the advection-dispersion model is applied in the first place to interpret the electromigration experimental results. The modelling results also show that Se(IV) species migrate relatively slow in comparison with iodide ions which is attributed to their smaller effective diffusion coefficient due to larger and unsymmetrical dissension. Our analysis also shows that both iodide and Se(IV) species should be considered as non-sorbing ions when transporting through the intact rock sample.

The work summarised here covers both sorption and diffusion aspects which are the two most important mechanisms that can retard the migration of radionuclides from a nuclear waste repository in the groundwater system of the bedrock. However, the work is just the beginning of a series of studies and leaves many questions behind. For example, the multi-site surface complexation model uses different mechanistic uptake processes to describe sorption, while the exact nature of the surface binding sites and surface complexes remains unknown. In order to check the "strong/weak sorption sites" hypothesis, structural information for the ions sorbed at the mineral-water surface should be studied. This kind of information can be provided by spectroscopic characterization techniques like XAS including EXAFS and XANES. We have assessed that the electromigration technique is a fast and simple method to obtain $D_e$ values of iodide and Se(IV) species. However, further application of the technique for strongly sorptive cations in variable groundwater conditions should be performed to explore the limitations of the technique. In addition, the reactive transport model should be further studied and better implemented to construct more confidence for the parameter evaluation.

# References


Alonso, U., Missana, T., Patelli, A., Ceccato, D., Albarran, N., García-Gutiérrez, M., Lopez-Torrubia, T., Rigato, V., 2009. Quantification of Au nanoparticles retention on a heterogeneous rock surface. Colloids and Surfaces A: Physicochemical and Engineering Aspects, Interfaces Against Pollution 347, 230–238. https://doi.org/10.1016/j.colsurfa.2009.04.046

André, M., Malmström, M.E., Neretnieks, I., 2009. Determination of sorption properties of intact rock samples: New methods based on electromigration. Journal of Contaminant Hydrology 103, 71–81. https://doi.org/10.1016/j.jconhyd.2008.09.006

André, Magnus, Neretnieks, I., Malmström, M.E., 2009. Measuring sorption coefficients and BET surface areas on intact drillcore and crushed granite samples. Radiochimica Acta International journal for chemical aspects of nuclear science and technology 96, 673–677. https://doi.org/10.1524/ract.2008.1552

Appelo, C.A.J., Postma, D., 2004. Geochemistry, Groundwater and Pollution. CRC Press.

Atwood, D.A., 2010. Radionuclides in the Environment. WILEY.

Baeyens, B., Bradbury, M.H., 1997. A mechanistic description of Ni and Zn sorption on Na-montmorillonite Part I: Titration and sorption measurements. Journal of Contaminant Hydrology 27, 199–222. https://doi.org/10.1016/S0169-7722(97)00008-9

Beauwens, T., De Cannière, P., Moors, H., Wang, L., Maes, N., 2005. Studying the migration behaviour of selenate in Boom Clay by electromigration. Engineering Geology, Electrokinetic Remediation - EREM 2003 77, 285–293. https://doi.org/10.1016/j.enggeo.2004.07.019

Bower, W.R., Morris, K., Livens, F.R., Mosselmans, J.F.W., Fallon, C.M., Fuller, A.J., Natrajan, L., Boothman, C., Lloyd, J.R., Utsunomiya, S., Grolimund, D., Ferreira Sanchez, D., Jilbert, T., Parker, J., Neill, T.S., Law, G.T.W., 2019. Metaschoepite Dissolution in Sediment Column Systems—Implications for Uranium Speciation and Transport. Environ. Sci. Technol. 53, 9915–9925. https://doi.org/10.1021/acs.est.9b02292

Bradbury, M.H., Baeyens, B., 2009a. Sorption modelling on illite. Part II: Actinide sorption and linear free energy relationships. Geochimica et Cosmochimica Acta 73, 1004–1013. https://doi.org/10.1016/j.gca.2008.11.016

Bradbury, M.H., Baeyens, B., 2009b. Sorption modelling on illite Part I: Titration measurements and the sorption of Ni, Co, Eu and Sn. Geochimica et Cosmochimica Acta 73, 990–1003. https://doi.org/10.1016/j.gca.2008.11.017

Bradbury, Michael H., Baeyens, B., 2005. Modelling the sorption of Mn(II), Co(II), Ni(II), Zn(II), Cd(II), Eu(III), Am(III), Sn(IV), Th(IV), Np(V) and U(VI) on montmorillonite: Linear free energy relationships and estimates of surface binding constants for some selected heavy metals and actinides. Geochimica et Cosmochimica Acta 69, 875–892. https://doi.org/10.1016/j.gca.2004.07.020

Bradbury, M. H., Baeyens, B., 2005. Experimental and Modelling Investigations on Na-Illite: Acid-Base Behaviour and the Sorption of Strontium, Nickel, Europium and Urany. Paul Scherrer Institut, Villigen PSI.

Bradbury, M.H., Baeyens, B., 2002. Sorption of Eu on Na- and Ca-montmorillonites: experimental investigations and modelling with cation exchange and surface complexation. Geochimica et Cosmochimica Acta 66, 2325–2334. https://doi.org/10.1016/S0016-7037(02)00841-4

Bradbury, M.H., Baeyens, B., 1995. A Quantitative Mechanistic Description of Ni, Zn and Ca Sorption on Na-Montmorillonite Part III: Modelling. TECHNICAL REPORT NTB 95-06, Nagra, Wettingen, Switzerland.

Bray, A.W., Benning, L.G., Bonneville, S., Oelkers, E.H., 2014. Biotite surface chemistry as a function of aqueous fluid composition. Geochimica et Cosmochimica Acta 128, 58–70. https://doi.org/10.1016/j.gca.2013.12.002

Bruggeman, C., Maes, A., Vancluysen, J., Vandemussele, P., 2005. Selenite reduction in Boom clay: Effect of FeS2, clay minerals and dissolved organic matter. Environmental Pollution 137, 209–221. https://doi.org/10.1016/j.envpol.2005.02.010

Carslaw, H.S., Jaeger, J.C., 1959. Conductin of Heat in Solids. Oxford at the Clarendon Press.

Clark, S.J., Segall, M.D., Pickard, C.J., Hasnip, P.J., Probert, M.I.J., Refson, K., Payne, M.C., 2009. First principles methods using CASTEP. Zeitschrift für Kristallographie - Crystalline Materials 220, 567–570. https://doi.org/10.1524/zkri.220.5.567.65075

Cordfunke, E.H.P., Konings, R.J.M., 1988. Chemical interactions in water-cooled nuclear fuel: A thermochemical approach. Journal of Nuclear Materials 152, 301–309. https://doi.org/10.1016/0022-3115(88)90341-8

Crank, J., 1979. The Mathematics of Diffusion. Clarendon Press.

Cronenberg, A.W., Osetek, D.J., 1987. Fuel morphology effects on the chemical form of iodine release from severely damaged fuel. Journal of Nuclear Materials 149, 252–260. https://doi.org/10.1016/0022-3115(87)90484-3

Dagnelie, R.V.H., Rasamimanana, S., Blin, V., Radwan, J., Thory, E., Robinet, J.-C., Lefèvre, G., 2018. Diffusion of organic anions in clay-rich media: Retardation and effect of anion exclusion. Chemosphere 213, 472–480. https://doi.org/10.1016/j.chemosphere.2018.09.064

Dash, B., Rath, S.S., 2020. Density Functional Theory and Molecular Dynamics insights into the site-dependent adsorption of hydrogen fluoride on kaolinite. Journal of Molecular Liquids 299, 112265. https://doi.org/10.1016/j.molliq.2019.112265

Davis, J.A., Kent, D.B., 1990. Surface Energy and Adsorption at Mineral/Water Interfaces: An Introduction. Mineral-Water Interface Geochemistry, Reviews in Mineralogy 23, 177–260.

De Cannière, P., Maes, A., Williams, S., Bruggeman, C., Beauwens, T., Maes, N., Cowper, M., 2010. Behaviour of Selenium in Boom Clay. SCK•CEN-ER-120.

de Hoog, F.R., Knight, J.H., Stokes, A.N., 1982. An Improved Method for Numerical Inversion of Laplace Transforms. SIAM Journal on Scientific and Statistical Computing 3, 357–366. https://doi.org/10.1137/0903022

Dohrmann, R., 2006. Problems in CEC determination of calcareous clayey sediments using the ammonium acetate method. Journal of Plant Nutrition and Soil Science 169, 330–334. https://doi.org/10.1002/jpln.200621975

Dzombak, D.A., Morel, F.M.M., 1990. Surface Complexation Modeling: Hydrous Ferric Oxide. John Wiley & Sons.

Ervanne, H., Hakanen, M., Lehto, J., 2016. Selenium sorption on clays in synthetic groundwaters representing crystalline bedrock conditions. J Radioanal Nucl Chem 307, 1365–1373. https://doi.org/10.1007/s10967-015-4254-7

Essington, M.E., 2015. Soil and Water Chemistry: An Integrative Approach. CRC Press.

Ewing, R.C., 2015. Long-term storage of spent nuclear fuel. Nature Materials 14, 252–257.

Gabos, M.B., Goldberg, S., Alleoni, L.R.F., 2014. Modeling selenium (IV and VI) adsorption envelopes in selected tropical soils using the constant capacitance model. Environmental Toxicology and Chemistry 33, 2197–2207. https://doi.org/10.1002/etc.2574

García-Gutiérrez, M., Cormenzana, J.L., Missana, T., Mingarro, M., Martín, P.L., 2006. Large-scale laboratory diffusion experiments in clay rocks. Physics and Chemistry of the Earth, Parts A/B/C, MIGRATION 2005, The 10th international conference on the chemistry

and migration of actinides and fission products in the geosphere 31, 523–530. https://doi.org/10.1016/j.pce.2006.04.004
Goldberg, S., Lesch, S.M., Suarez, D.L., 2007. Predicting selenite adsorption by soils using soil chemical parameters in the constant capacitance model. Geochimica et Cosmochimica Acta, Physical Chemistry of Soils and Aquifers: A Special Issue in Honor of Garrison Sposito 71, 5750–5762. https://doi.org/10.1016/j.gca.2007.04.036
Hayes, K.F., Roe, A.L., Brown, G.E., Hodgson, K.O., Leckie, J.O., Parks, G.A., 1987. In Situ X-ray Absorption Study of Surface Complexes: Selenium Oxyanions on α-FeOOH. Science 238, 783–786. https://doi.org/10.1126/science.238.4828.783
He, Y., Xiang, Y., Zhou, Y., Yang, Y., Zhang, J., Huang, H., Shang, C., Luo, L., Gao, J., Tang, L., 2018. Selenium contamination, consequences and remediation techniques in water and soils: A review. Environmental Research 164, 288–301. https://doi.org/10.1016/j.envres.2018.02.037
Hjerpe, T., Ikonen, A.T.K., Broed, R., 2010. Biosphere assessment report 2009 (No. Posiva 2010-03). Posiva Oy, Olkiluoto.
IAEA International Atomic Energy Agency, 2018a. Nuclear Power Reactors in the World. Reference Data Series No.2 (2018 Edition).
IAEA International Atomic Energy Agency, 2018b. Status and Trends in Spent Fuel and Radioactive Waste Management. IAEA Nuclear Energy Series No. NW-T-1.14.
Ikonen, J., Voutilainen, M., Söderlund, M., Jokelainen, L., Siitari-Kauppi, M., Martin, A., 2016. Sorption and diffusion of selenium oxyanions in granitic rock. J Contam Hydrol 192, 203–211. https://doi.org/10.1016/j.jconhyd.2016.08.003
James, R.O., Healy, T.W., 1972. Adsorption of hydrolyzable metal ions at the oxide—water interface. I. Co(II) adsorption on SiO2 and TiO2 as model systems. Journal of Colloid and Interface Science 40, 42–52. https://doi.org/10.1016/0021-9797(72)90172-5
Kelokaski, M., Siitari-Kauppi, M., Sardini, P., Möri, A., Hellmuth, K.H., 2006. Characterisation of pore space geometry by 14C-PMMA impregnation—development work for in situ studies. Journal of Geochemical Exploration 90, 45–52. https://doi.org/10.1016/j.gexplo.2005.09.005
Kuva, J., Voutilainen, M., Kekäläinen, P., Siitari-Kauppi, M., Sammaljärvi, J., Timonen, J., Koskinen, L., 2016. Gas Phase Measurements of Matrix Diffusion in Rock Samples from Olkiluoto Bedrock, Finland. Transport in Porous Media 115, 1–20. https://doi.org/10.1007/s11242-016-0748-1
Kuva, J., Voutilainen, M., Kekäläinen, P., Siitari-Kauppi, M., Timonen, J., Koskinen, L., 2015. Gas Phase Measurements of Porosity, Diffusion Coefficient, and Permeability in Rock Samples from Olkiluoto Bedrock, Finland. Transport in Porous Media 107, 187–204. https://doi.org/10.1007/s11242-014-0432-2
Leach, A.R., 2001. Molecular Modelling: Principles and Applications, 2nd ed. Pearson Education.
Lehto, J., Hou, X., 2011. Chemistry and Analysis of Radionuclides Laboratory Techiques and Methodology. WILEY-VCH.
Li, X., Puhakka, E., Ikonen, J., Söderlund, M., Lindberg, A., Holgersson, S., Martin, A., Siitari-Kauppi, M., 2018. Sorption of Se species on mineral surfaces, part I: Batch sorption and multi-site modelling. Applied Geochemistry 95, 147–157. https://doi.org/10.1016/j.apgeochem.2018.05.024
Li, X., Puhakka, E., Liu, L., Zhang, W., Ikonen, J., Lindberg, A., Siitari-Kauppi, M., 2020. Multi-site surface complexation modelling of Se(IV) sorption on biotite. Chemical Geology 533, 119433. https://doi.org/10.1016/j.chemgeo.2019.119433

Li, Z., Liang, D., Peng, Q., Cui, Z., Huang, J., Lin, Z., 2017. Interaction between selenium and soil organic matter and its impact on soil selenium bioavailability: A review. Geoderma 295, 69–79. https://doi.org/10.1016/j.geoderma.2017.02.019

Liu, J., Löfgren, M., Neretnieks, I., 2006. Data and uncertainty assessment Matrix diffusivity and porosity in situ. Department of Chemical Engineering and Technology, Royal Institute of Technology, KTH.

Löfgren, M., 2005. Diffusive properties of granitic rock as measured by in-situ electrical methods. Department of Chemical Engineering and Technology. Royal Institute of Technology, Stockholm, Sweden.

Löfgren, M., Neretnieks, I., 2006. Through-electromigration: A new method of investigating pore connectivity and obtaining formation factors. Journal of Contaminant Hydrology 87, 237–252. https://doi.org/10.1016/j.jconhyd.2006.05.006

Maes, N., Moors, H., Dierckx, A., De Cannière, P., Put, M., 1999. The assessment of electromigration as a new technique to study diffusion of radionuclides in clayey soils. Journal of Contaminant Hydrology 36, 231–247. https://doi.org/10.1016/S0169-7722(98)00146-6

Maes, N., Moors, H., Wang, L., Delècaut, G., De Cannière, P., Put, M., 2002. The use of electromigration as a qualitative technique to study the migration behaviour and speciation of uranium in the Boom Clay. Radiochimica Acta 90. https://doi.org/10.1524/ract.2002.90.9-11_2002.741

Mattsson, K.-J., Rauséus, G., Eklund, S., 2007. Oskarshamn site investigation. Boremap mapping of core drilled DFN boreholes KLX11B–KLX11F. SKB report, P-06-244.

Missana, T., Alonso, U., Scheinost, A.C., Granizo, N., García-Gutiérrez, M., 2009. Selenite retention by nanocrystalline magnetite: Role of adsorption, reduction and dissolution/co-precipitation processes. Geochimica et Cosmochimica Acta 73, 6205–6217. https://doi.org/10.1016/j.gca.2009.07.005

Mitchell, J.K., Soga, K., 2005. Fundamentals of soil behavior. John Wiley & Sons.

Möri, A., Alexander, W.R., Geckeis, H., Hauser, W., Schäfer, T., Eikenberg, J., Fierz, Th., Degueldre, C., Missana, T., 2003. The colloid and radionuclide retardation experiment at the Grimsel Test Site: influence of bentonite colloids on radionuclide migration in a fractured rock. Colloids and Surfaces A: Physicochemical and Engineering Aspects 217, 33–47. https://doi.org/10.1016/S0927-7757(02)00556-3

Muuri, E., Ikonen, J., Matara-aho, M., Lindberg, A., Holgersson, S., Voutilainen, M., Siitari-Kauppi, M., Martin, A., 2016. Behavior of Cs in Grimsel granodiorite: sorption on main minerals and crushed rock. Radiochimica Acta 104, 575–582. https://doi.org/10.1515/ract-2016-2574

Muuri, E., Sorokina, T., García, D., Grivé, M., Bruno, J., Koskinen, L., Martin, A., Siitari-Kauppi, M., 2018. The in-diffusion of 133Ba in granitic rock cubes from the Olkiluoto and Grimsel in-situ test sites. Applied Geochemistry 92, 188–195. https://doi.org/10.1016/j.apgeochem.2018.03.011

National Institute of Advanced Industrial Science and Technology, 2005. Eh_pH_Diagrams, Intercomparison of thermodynamic databases, Geological Survey of Japan Open File Report No.419.

Neall, F., Pastina, B., Smith, P., Gribi, P., Snellman, M., Johnson, L., 2007. Safety assessment for a KBS-3H spent nuclear fuel repository at Olkiluoto: complementary evaluations of safety report (No. Posiva 2007-10). Posiva Oy, Olkiluoto.

Neretnieks, I., 1980. Diffusion in the rock matrix: An important factor in radionuclide retardation? Journal of Geophysical Research: Solid Earth 85, 4379–4397. https://doi.org/10.1029/JB085iB08p04379

Ohlsson, Y., 2000. Studies of ionic diffusion in crystalline rock (Doctoral thesis). Royal Institute of Technology, Stockholm, Sweden.
Posiva Oy, 2013. Safety case for the disposal of spent nuclear fuel at Olkiluoto. Models and data for the repository system 2012. Parts 1 and 2. Posiva Oy, POSIVA Report 2013-1.
Posiva Oy, 2012. Safety Case for the Disposal of Spent Nuclear Fuel at Olkiluoto- Features, Events and Processes 2012. Posiva Reoprt 2012-07.
Puhakka, E., Li, X., Ikonen, J., Siitari-Kauppi, M., 2019. Sorption of selenium species onto phlogopite and calcite surfaces: DFT studies. Journal of Contaminant Hydrology 227, 103553. https://doi.org/10.1016/j.jconhyd.2019.103553
Puhakka, E., Ritala, M., Lehto, J., 2020. Effect of potassium for cesium replacement in atomic level structure of potassium cobalt hexacyanoferrate(II). Radiochimica Acta 108, 451–457. https://doi.org/10.1515/ract-2019-3165
Puukko, E., 2014. Sorption of cesium in intact rock. Posiva Oy, Posiva Report 2014-13.
Puukko, E., Lehto, J., Lindberg, A., Voutilainen, M., 2018. Electromigration experiments for studying transport parameters and sorption of cesium and strontium on intact crystalline rock. Journal of Contaminant Hydrology 217, 1–7. https://doi.org/10.1016/j.jconhyd.2018.08.010
Sarkar, D., Essington, M.E., Misra, K.C., 2000. Adsorption of Mercury(II) by Kaolinite. Soil Science Society of America Journal 64, 1968. https://doi.org/10.2136/sssaj2000.6461968x
Sarkar, D., Essington, M.E., Misra, K.C., 1999. Adsorption of Mercury(II) by Variable Charge Surfaces of Quartz and Gibbsite. Soil Science Society of America Journal 63, 1626. https://doi.org/10.2136/sssaj1999.6361626x
Siegel, M., Bryan, C., 2003. Environmental Geochemistry of Radioactive Contamination (No. SAND2003-2063). SANDIA REPORT, SAND2003-2063.
SKB, 2013. Äspö Hard Rock Laboratory Annual report 2012. Technical Report: TR-13-10.
SKB, 1999. Deep repository for spent nuclear fuel SR 97 - Post-closure safety Main Report Volume I. Technical Report TR-99-06.
Smith, P., Neall, F., Snellman, M., Pastina, B., Nordman, H., Johnson, L., Hjerpe, T., 2007. Safety assessment for a KBS-3H spent nuclear fuel repository at Olkiluoto: summary report. Posiva Report, Posiva 2007-06.
Soler, J.M., Landa, J., Havlova, V., Tachi, Y., Ebina, T., Sardini, P., Siitari-Kauppi, M., Eikenberg, J., Martin, A.J., 2015. Comparative modeling of an in situ diffusion experiment in granite at the Grimsel Test Site. Journal of Contaminant Hydrology 179, 89–101. https://doi.org/10.1016/j.jconhyd.2015.06.002
Sudicky, E.A., Frind, E.O., 1982. Contaminant transport in fractured porous media: Analytical solutions for a system of parallel fractures. Water Resources Research 18, 1634–1642. https://doi.org/10.1029/WR018i006p01634
Tachi, Y., Ebina, T., Takeda, C., Saito, T., Takahashi, H., Ohuchi, Y., Martin, A.J., 2015. Matrix diffusion and sorption of Cs+, Na+, I– and HTO in granodiorite: Laboratory-scale results and their extrapolation to the in situ condition. Journal of Contaminant Hydrology 179, 10–24. https://doi.org/10.1016/j.jconhyd.2015.05.003
Tang, D.H., Frind, E.O., Sudicky, E.A., 1981. Contaminant transport in fractured porous media: Analytical solution for a single fracture. Water Resources Research 17, 555–564. https://doi.org/10.1029/WR017i003p00555
Watts, H.D., O'Day, P.A., Kubicki, J.D., 2019. Gibbsite (100) and Kaolinite (100) Sorption of Cadmium(II): A Density Functional Theory and XANES Study of Structures and Energies. J. Phys. Chem. A 123, 6319–6333. https://doi.org/10.1021/acs.jpca.9b05159

Wigeland, R.A., Bauer, T.H., Fanning, T.H., Morris, E.E., 2004. Spent Nuclear Fuel Separation and Transmutation Criteria for Benefit to a Geologic Repository. Waste Management 2004 Conference, Tucson, USA.

Yang, X., Ge, X., He, J., Wang, C., Qi, L., Wang, X., Liu, C., 2018. Effects of Mineral Compositions on Matrix Diffusion and Sorption of $^{75}$ Se(IV) in Granite. Environmental Science & Technology 52, 1320–1329. https://doi.org/10.1021/acs.est.7b05795